Editors' Suggestion

Vibrational excitation in the e+CO_2 system: Nonlocal model of $\Sigma\Pi$ vibronic coupling through the continuum

Jan Dvořák,* Karel Houfek,† and Martin Čížek‡

Charles University, Faculty of Mathematics and Physics, Institute of Theoretical Physics, V Holešovičkách 2, 180 00 Prague 8, Czech Republic

(Received 11 February 2022; accepted 20 May 2022; published 27 June 2022)

We present our model of the e+CO_2 system that has been used to calculate the two-dimensional electron energy-loss spectrum of CO_2 for incoming electron energies up to 5 eV reported in our Letter [Phys. Rev. Lett. **129**, 013401 (2022)]. We derive the effective Hamiltonian that describes the nonlocal dynamics of CO_2^- within the full vibrational space and in the presence of the $^2\Sigma_g^+$ virtual state and the Renner-Teller coupled $^2\Pi_u$ shape resonance. The electronic states are represented by three discrete states that interact directly with each other and also indirectly through the electronic continuum that consists of s and p partial waves. Based on our *ab initio* fixed-nuclei R-matrix calculations, parameters of the model are determined using a fitting procedure that utilizes the high symmetry of the system. The topology of the resulting complex potential energy surfaces is discussed. The model is constructed in such a way that the Hamiltonian expressed in a harmonic vibrational basis of the neutral molecule is a sparse matrix which enabled us to solve the multidimensional dynamics of vibrational excitation using iterative methods based on Krylov subspaces.

DOI: 10.1103/PhysRevA.105.062821

I. INTRODUCTION

The model of the discrete state in continuum has been used for the description of inelastic electron-molecule collisions for a long time [1]. The most natural application of the model is to narrow resonances where the finite lifetime of a compound electron-molecule state is directly related to the negative imaginary part of the potential [2]. In such cases, the model is known as the local-complex-potential (LCP) approximation or the boomerang model [3]. However, a more elaborate form of the theory with a nonlocal and energy-dependent effective potential is necessary in systems where a bound anionic state disappears in the continuum when the molecular geometry is deformed without becoming a clear resonance [4]. The importance of nonlocal effects has been recognized by Cederbaum and Domcke [5], who were also the first to solve the full nonlocal version of the dynamics for harmonic molecular potentials using the continuous fraction method [6]. Later the nonlocal dynamics was numerically solved also for realistic *ab initio* potentials of diatomic molecules leading to a good correspondence with experimental data; see, for example, Ref. [7] and references therein.

In the application of the nonlocal approach to polyatomic molecules, we face numerous challenges including the presence of much more parameters for the construction of such models and a more difficult treatment of the dynamics. The interaction of multiple anionic states is also more often involved in polyatomics. Triatomic molecules already represent a very challenging problem, for which, however, a nearly complete solution of the dynamics may be hoped for. A large step in this direction within the LCP approximation has been done for the electron scattering from CO_2 [8,9], H_2O (see Haxton *et al.* [10,11] and references therein), and HCN [12,13]. In the case of water and carbon dioxide molecules, authors even treated the nonadiabatic coupling of multiple metastable states. Although the LCP approximation correctly captures many features, its limitations in the case of the H_2O molecule have been pointed out in Ref. [11]. To the best of our knowledge only two works extend the calculations for polyatomic molecules beyond the LCP approximation and take into account more than one vibrational degree of freedom. Recently, Abalampitiya and Fabrikant [14] treated the dissociative attachment to the CF_3Cl molecule through a single discrete anionic state within the nonlocal theory with two relevant vibrational degrees of freedom. The full nonlocal vibronic dynamics of two discrete states and two vibrational modes was discussed for a model Hamiltonian by Estrada *et al.* [15]. Further generalization of this model with examples for specific molecules were discussed by Feuerbacher *et al.* [16,17], but they focused on only static aspects of the potential energy surfaces and made no attempts to solve the dynamics.

We extend the approach of Estrada *et al.* [15] to the case of three electronic states of a linear triatomic molecule and four vibrational coordinates. We apply it to vibrational excitation of the CO_2 molecule by slow electrons. Since our work is rather extensive, we discuss it in three papers. Main results of our calculations together with new experimental data measured by our colleagues are presented in Ref. [18], where we propose our interpretation of the two-dimensional electron energy-loss spectrum of CO_2. Here we describe the theoretical model, its construction from *ab initio* data, and a procedure how to solve the dynamics. The third paper (a follow-up to

*Jan.Dvorak@utf.mff.cuni.cz
†Karel.Houfek@mff.cuni.cz
‡Martin.Cizek@mff.cuni.cz

this one) will focus on a detailed comparison and discussion of the theoretical and experimental results.

There is an extensive literature on theoretical description of vibrational excitation of the CO_2 molecule. We will review the previous works in more detail in a follow-up to this paper. Here we would like to mention few works that affected our choice of the particular form of the model. The electron scattering off CO_2 up to about 2 eV is dominated by the $^2\Sigma_g^+$ virtual state [19–21]. For energies around 4 eV Boness and Schulz [22] observed a boomerang structure in their vibrational excitation cross sections, which they attributed to a $^2\Pi_u$ shape resonance.

The near-threshold region was studied by Whitten and Lane [23] and Mazevet *et al.* [24]. Estrada and Domcke [25] performed one-dimensional (1D) calculations in symmetric stretching using the discrete-state-in-continuum model to study the effect of the virtual state. The most advanced treatment of the near threshold region so far has been the effective-range-potential model of combined excitation of symmetric stretching and bending by Vanroose *et al.* [26]. The theoretical treatment of the $^2\Pi_u$ shape resonance also involves works of different complexity. We would like to mention the 1D description of the origin of boomerang oscillations by Čadež *et al.* [27] and 2D LCP studies by Kazansky and Sergeeva [28,29] and Rescigno *et al.* [8] who included both the symmetric stretching and bending, even based on *ab initio* fixed-nuclei data in the latter case. Finally, McCurdy *et al.* [9] improved the description even further by considering the Renner-Teller splitting of the $^2\Pi_u$ resonance.

The $^2\Sigma_g^+$ and $^2\Pi_u$ states have been treated separately in all previous theoretical works. It is well known that the potential of the ground state of CO_2^- possesses a minimum in C_{2v} geometry [30,31] and *ab initio* calculations of Resigno *et al.* [32] indicated that the minimum is connected to the $^2\Pi_u$ shape resonance through the lower Renner-Teller component. On the other hand, *R*-matrix calculations of Morgan *et al.* [21,33] showed that the virtual state becomes bound upon bending too; see also the discussion in the introduction of Vanroose *et al.* [34], who tried to provide an insight into this problem using an analytically solvable scattering model. Sommerfeld [35] reported that when a very diffuse basis is used, the potential energy of the ground state of CO_2^- behaves qualitatively differently than the earlier calculations [30,31] had shown. The potential does not monotonically rise along the trajectory from the minimum to the autodetachment region but it drops before reaching the crossing point with the neutral potential, and then it crosses or rather merges with the neutral potential. On top of that, Sommerfeld *et al.* [36] argued that the minimum is connected to the virtual state which mixes with the lower Renner-Teller component as the molecule bends [37]. Hence, they suggested that the low-energy scattering off CO_2 should be treated as a coupled nonlocal problem of the $^2\Sigma_g^+$ and $^2\Pi_u$ states. In this paper we present our attempt to construct such a model.

The paper is organized as follows. In Sec. II we review basic ideas of the nonlocal model for the description of vibrational excitation by electron impact in the case of multiple interacting discrete states and several vibrational degrees of freedom. Then we apply the approach to the $^2\Sigma_g^+$ and $^2\Pi_u$ states of CO_2^- taking into account all vibrational modes. We show how the $D_{\infty h}$ symmetry of the system restricts the model structure. Section III represents a preparation stage for the model construction from *ab initio* data. We describe there the relation of diabatic and adiabatic representations within the model and the effect of gradual lowering of the molecular symmetry on fixed-nuclei scattering quantities. In Sec. IV we first describe our *ab initio* fixed-nuclei *R*-matrix calculations and then we focus on obtaining model parameters from these data using a least-squares fitting procedure. The quality and interpretation of the resulting model is discussed in Sec. V. Finally, Sec. VI is devoted to numerical details considering the evaluation of the nonlocal Hamiltonian and solution of the dynamics. We conclude in Sec. VII by summarizing the results and discussing possible future improvements of the present concept for the application to other molecular systems.

II. VIBRONIC COUPLING MODEL

The model is based on work by Estrada *et al.* [15] who generalized the original vibronic coupling model for bound states [38] to the case of short-lived states. They described a polyatomic system with two anionic discrete states of different symmetries and two vibrational degrees of freedom. The discrete states were coupled only directly through a nontotally symmetric vibrational mode since the coupling with the electronic continuum was considered independent of vibrational coordinates. Here we extend their approach in two ways. The general vibronic coupling scheme in linear molecules as discussed by Köppel *et al.* [37] is used for the direct coupling of three discrete electronic states considering all vibrational modes of a linear triatomic molecule. Moreover, we apply the same scheme to the vibronic coupling of the discrete states with the continuum.

A. General discrete-states-in-continuum model

The key assumption of the model is that vibrational excitation of a molecule is mediated by a small number of metastable anionic discrete states that are formed by the attachment of an incoming electron to the neutral molecule. The effective Hamiltonian for the dynamics within the discrete-state space is then derived using the projection-operator formalism of Feshbach [39].

The electronic Hilbert space of the electron-molecule system is separated into a discrete-state (or resonant)[1] subspace and a background continuum subspace. We define the projection operator on the discrete-state subspace by

$$\mathcal{Q} = \sum_d |d\rangle\langle d|, \tag{1}$$

where d runs over all included discrete states. The complementary operator

$$\mathcal{P} = \mathcal{I} - \mathcal{Q}, \tag{2}$$

[1]Since the discrete states involved in the context of electron-molecule collisions are not limited to resonances, this term caused some confusion in the past. We will mostly use the term discrete state instead of resonance.

where $\mathcal{I}$ is the identity operator, then projects on the background continuum part. The discrete states $|d\rangle$ thus form a basis in the discrete-state part of the electronic Hilbert space. The basis $|\epsilon\mu\rangle$ of the continuum part is chosen to diagonalize the fixed-nuclei electronic Hamiltonian $\mathscr{H}_{\rm el}$ projected on the background space

$$\mathcal{P}\mathscr{H}_{\rm el}\mathcal{P}|\epsilon\mu\rangle = [V_0 + \epsilon]|\epsilon\mu\rangle, \tag{3}$$

where ϵ and μ denote energy and additional quantum numbers identifying the electronic states in the continuum. As a result, $\mathscr{H}_{\rm el}$ can be formally written as the following infinite matrix:

$$\mathscr{H}_{\rm el} = V_0\mathcal{I} + \left(\begin{array}{c|ccc} U & \multicolumn{3}{c}{V_\epsilon} \\ \hline & \ddots & & \\ V_\epsilon^\dagger & & \epsilon & \\ & & & \ddots \end{array}\right), \tag{4}$$

where V_0 is the potential energy surface of the neutral molecule, $U = \mathcal{Q}(\mathscr{H}_{\rm el} - V_0\mathcal{I})\mathcal{Q}$ is a matrix describing the discrete-state energies relative to the threshold V_0 (diagonal elements) and also the direct interaction among the discrete states (off-diagonal elements), and $V_\epsilon = \mathcal{Q}\mathscr{H}_{\rm el}\mathcal{P}$ represents the interaction of the discrete states with the electronic continuum states.

The potential energy $V_0(\vec{q}\,)$ and all matrix elements $U_{dd'}(\vec{q}\,) = \langle d|U|d'\rangle$, $V^\mu_{d\epsilon}(\vec{q}\,) = \langle d|V_\epsilon|\epsilon\mu\rangle$ depend on nuclear coordinates $\vec{q}$. The vibrational motion is included into the dynamics by adding the kinetic energy operator T_N for nuclei to $\mathscr{H}_{\rm el}$. The electronic continuum is eliminated by the projection-operator formalism of Feshbach [39], which assumes the diabaticity of the full basis $|d\rangle$, $|\epsilon\mu\rangle$. It means that all sharp features in the dependence on the molecular geometry $\vec{q}$ such as resonances or virtual states have to be eliminated from the continuum $|\epsilon\mu\rangle$ by the choice of the discrete states. As a consequence of the diabaticity, the projection operators $\mathcal{Q}$ and $\mathcal{P}$ commute with the kinetic energy operator T_N. Then the vibrational dynamics of the electron-molecule collision process is reduced to the electronic discrete-state subspace $\mathcal{Q}$ only. For details we refer the reader to reviews [40,41] which treat the system with only one discrete state but the generalization to more states is straightforward.

The effective Hamiltonian for the vibrational motion of the molecular anion reads

$$H = H_0\mathbb{1} + U + F(E - H_0), \tag{5}$$

where $H_0 = T_N + V_0$ is the vibrational Hamiltonian of the neutral molecule, $\mathbb{1}$ is the unit operator in the discrete-state subspace, U is the same matrix as in Eq. (4), $F(E - H_0)$ is the level-shift operator resulting from the interaction with the continuum, and E denotes total energy of the system that is conserved during the process. Throughout this paper, we reserve the symbol E only for the total energy. Electron energy will be denoted by ϵ. The elements of the level-shift operator matrix are defined by the integrals

$$F_{dd'}(E - H_0) = \sum_\mu \int V^\mu_{d\epsilon}(E - H_0 - \epsilon + i\eta)^{-1} V^{\mu^*}_{d'\epsilon} d\epsilon, \tag{6}$$

where η is a positive infinitesimal. This operator is a matrix in the discrete-state indices d, d' and is also a nonlocal operator in the nuclear coordinates $\vec{q}$.

The discrete-state (resonant) contribution to the T matrix for vibrational excitation from the initial vibrational state v_i to the final state v_f is given by

$$T_{v_f\mu_f \leftarrow v_i\mu_i} = \langle v_f|V^{\mu_f\,\dagger}_{\epsilon_f}(E\mathbb{1} - H)^{-1}V^{\mu_i}_{\epsilon_i}|v_i\rangle, \tag{7}$$

where μ_i and μ_f denote the initial and final electron partial waves. The initial ϵ_i and final ϵ_f electron energies satisfy the conservation law

$$E = E_{v_i} + \epsilon_i = E_{v_f} + \epsilon_f \tag{8}$$

with internal vibrational energies E_{v_i}, E_{v_f} of the neutral molecule given by $H_0|v\rangle = E_v|v\rangle$. By solving the vibrational dynamics of the collision we mean the application of the matrix inversion $(E\mathbb{1} - H)^{-1}$ on the initial state. Details are given in Sec. VI, where the integral and differential cross sections obtained from the T matrix are also discussed.

B. Coordinates and states for e+CO_2 model

The discussion of the dynamics of the electron-molecule collision within the framework of the nonlocal model has been completely general so far. At this point we introduce details specific for the low-energy e+CO_2 collisions.

1. Normal vibrational coordinates

We describe nuclear configurations $\vec{q}$ of the molecule in terms of normal vibrational coordinates $\vec{q} = \{Q_i\}$. The CO_2 molecule is linear and symmetric in its equilibrium geometry. Thus, it has four vibrational modes: symmetric stretching, antisymmetric stretching, and two-dimensional bending. We denote the corresponding dimensionless normal coordinates by Q_g, Q_u, Q_x, and Q_y, respectively, which are defined in accordance with Witteman [42] in Appendix A. It is convenient to describe bending in terms of complex coordinates $Q_\pm = Q_x \pm iQ_y$. Moreover, it also becomes useful to use polar bending coordinates (ρ, φ) defined by

$$Q_x = \rho\cos\varphi, \quad Q_y = \rho\sin\varphi, \tag{9}$$

so that $Q_\pm = \rho e^{\pm i\varphi}$ and $\rho^2 = Q_x^2 + Q_y^2 = Q_+Q_-$.

We prefer to use normal coordinates measured in bohrs when we compare *ab initio* data with fixed-nuclei quantities obtained within the model. These coordinates are denoted by S_g, S_u, S_x, and S_y and are also defined in Appendix A. Finally, we denote the magnitude of bending by S_b which is defined by $S_b^2 = S_x^2 + S_y^2$.

2. Discrete electronic states

As discussed in the introduction, to capture the phenomena in the low-energy electron scattering with CO_2 we include both Renner-Teller components of the $^2\Pi_u$ shape resonance and the $^2\Sigma_g^+$ virtual state of CO_2^- in our discrete-state space. In the following discussion we simplify the notation and use $d \in \{\Pi_+, \Sigma, \Pi_-\}$ to identify the individual discrete states. These states are eigenstates of the projection of the electronic angular momentum operator on the molecular axis corresponding to eigenvalues $\hbar, 0, -\hbar$, respectively. Sometimes it is useful to work with real Cartesian components Π_x, Π_y, which are given by the relations $\Pi_\pm = (\Pi_x \pm i\Pi_y)/\sqrt{2}$.

Note that there is one more state of $^2\Pi_g$ symmetry in the energy window of interest, which connects to the $O^- + CO$ dissociative attachment channel [43]. We do not consider this state for two reasons. First, it would be very difficult to include the dissociative channel in our calculation with four vibrational degrees of freedom. Second, this channel is connected through a conical intersection that is not much permeable since the magnitude of the dissociative attachment cross section [44] is at least one order of magnitude smaller then the vibrational excitation cross section even at high-energy loss [22].

3. Continuum electronic states

In general, the projection operators $\mathcal{Q}$ and $\mathcal{P}$ defined by Eqs. (1) and (2) are totally symmetric. The background scattering problem Eq. (3) is therefore solved in the same symmetry as the original neutral molecule and we can label the background continuum states according to the irreducible representations of the $D_{\infty h}$ point group.

In order to describe primary features of the e+CO_2 dynamics, we have to include at least all four components of s and p electron partial waves. The $^2\Sigma_g^+$ virtual state at the equilibrium molecular geometry is observed in fixed-nuclei eigenphases of the Σ_g^+ symmetry. This includes partial waves (l, m) for even values of l and $m = 0$. We consider only the lowest partial wave of this symmetry, $(l, m) = (0, 0)$, in our model and we denote the respective continuum states by $|\epsilon\mu\rangle$ with $\mu = s$. Similarly, the $^2\Pi_u$ shape resonance at the equilibrium geometry is observed in the Π_u symmetry, which corresponds to partial waves with odd l and $m = \pm 1$. We again limit the model to the lowest allowed l, that is $l = 1$, and the continuum states are denoted by $|\epsilon\mu\rangle$ with $\mu = p+$ and $\mu = p-$. Finally, we want to describe excitation of one quantum of asymmetric stretching, which is of the Σ_u^+ symmetry. Since the molecule is originally in the totally symmetric state, the product of representations of the incoming and outgoing electrons have to contain the Σ_u^+ representation. The lowest partial waves allowing for this possibility is the combination of an s-wave and p_z-wave electron, i.e., $(l, m) = (1, 0)$. Therefore, we include continuum states $|\epsilon\mu\rangle$ with $\mu = p_z$ of the Σ_u^+ symmetry. To summarize, the continuum coupling matrix $V_\epsilon = \{V_{d\epsilon}^\mu\}$ is a 3×4 matrix in our model for three values of $d \in \{\Pi_+, \Sigma, \Pi_-\}$ and four values of $\mu \in \{s, p_z, p_+, p_-\}$. Once again, we also sometimes use Cartesian components p_x, p_y defined by the relations $p_\pm = (p_x \pm i p_y)/\sqrt{2}$.

C. Symmetry restrictions on U and V_ϵ matrices

Up to now, we have considered an arbitrary dependence of the U and V_ϵ matrices on the normal coordinates. At the equilibrium geometry, the CO_2 molecule has the symmetry given by the $D_{\infty h}$ point group, and therefore, the full Hamiltonian Eq. (4) and consequently also the effective Hamiltonian Eq. (5) and the matrices U and V_ϵ have to be invariant with respect to symmetry operations of the $D_{\infty h}$ group. This imposes strong restrictions on the possible dependence of individual matrix elements on the vibrational coordinates.

The discrete state Σ, symmetric stretching coordinate Q_g, and $|\epsilon s\rangle$ continuum states transform according to the Σ_g^+ representation of $D_{\infty h}$, the antisymmetric stretching coordinate Q_u and $|\epsilon p_z\rangle$ continuum states transform as Σ_u^+, and the discrete states $\Pi_\pm$, bending coordinates $Q_\pm$ and $|\epsilon p_\pm\rangle$ continuum states as Π_u. Let us denote either states or coordinates that transform according to the Σ_g^+, Σ_u^+, and Π_u representations by σ_g, σ_u, and $\pi_\pm$, respectively. The rotation C_α by an angle α around the molecular axis then gives [45]

$$C_\alpha \sigma_g = \sigma_g, \quad C_\alpha \sigma_u = \sigma_u, \quad C_\alpha \pi_\pm = e^{\pm i\alpha}\pi_\pm. \tag{10}$$

Similarly, the reflection $\sigma_{v\alpha}$ through the plane that contains the molecular axis (z axis) and is inclined by angle α with respect to the x axis acts as

$$\sigma_{v\alpha}\,\sigma_g = \sigma_g, \quad \sigma_{v\alpha}\,\sigma_u = \sigma_u, \quad \sigma_{v\alpha}\,\pi_\pm = e^{\pm 2i\alpha}\pi_\mp, \tag{11}$$

and finally, under the inversion I the states transform in the following way:

$$I\sigma_g = \sigma_g, \quad I\sigma_u = -\sigma_u, \quad I\pi_\pm = -\pi_\pm. \tag{12}$$

On top of that, the $D_{\infty h}$ group also contains rotations by 180° about lines that are perpendicular to the molecular axis and improper rotations around the molecular axis, but we do not need these operations to derive the form of the U and V_ϵ matrices.

We explicitly derive the dependence of the $U_{\Pi_+\Sigma} = \langle\Pi_+|U|\Sigma\rangle$ element on the normal coordinates. Under the rotation we get

$$C_\alpha(|\Pi_+\rangle U_{\Pi_+\Sigma}\langle\Sigma|) = e^{i\alpha}|\Pi_+\rangle(C_\alpha U_{\Pi_+\Sigma})\langle\Sigma|. \tag{13}$$

To compensate the factor $\exp(i\alpha)$, the $U_{\Pi_+\Sigma}$ element has to transform as the Q_- bending coordinate, that is $U_{\Pi_+\Sigma} = \lambda_1 Q_-$ where λ_1 can be a function of Q_g, Q_u, and totally symmetric combination $Q_+Q_- = \rho^2$. Similarly, we find out that $U_{\Pi_-\Sigma} = \langle\Pi_-|U|\Sigma\rangle = \lambda_2 Q_+$. Under the reflection we have

$$\sigma_{v\alpha}(|\Pi_+\rangle U_{\Pi_+\Sigma}\langle\Sigma|) = e^{-2i\alpha}|\Pi_-\rangle(\sigma_{v\alpha}\,U_{\Pi_+\Sigma})\langle\Sigma|, \tag{14}$$

which leads to the following condition:

$$e^{-2i\alpha}(\sigma_{v\alpha}\,U_{\Pi_+\Sigma}) = U_{\Pi_-\Sigma}, \tag{15}$$

which implies $\lambda_1 = \lambda_2 \equiv \lambda$. Finally, the Q_- coordinate also compensates the sign change under the inversion

$$I(|\Pi_+\rangle U_{\Pi_+\Sigma}\langle\Sigma|) = -|\Pi_+\rangle(IU_{\Pi_+\Sigma})\langle\Sigma|, \tag{16}$$

hence, the function λ can not depend on odd powers of Q_u. In the end, we have $U_{\Pi_+\Sigma} = \lambda Q_-$ and $U_{\Pi_-\Sigma} = \lambda Q_+$, where λ is an arbitrary function of totally symmetric combinations of the normal coordinates, that is, a function of Q_g, Q_u^2, and Q_+Q_-.

By performing the symmetry analysis for the remaining elements of U, we get

$$U = \begin{array}{c} \\ \Pi_+ \\ \Sigma \\ \Pi_- \end{array} \begin{array}{c} \begin{array}{ccc} \Pi_+ & \Sigma & \Pi_- \end{array} \\ \begin{pmatrix} E_\Pi & \lambda Q_- & \xi Q_-^2 \\ \lambda Q_+ & E_\Sigma & \lambda Q_- \\ \xi Q_+^2 & \lambda Q_+ & E_\Pi \end{pmatrix} \end{array}, \tag{17}$$

where E_Π, E_Σ, λ, and ξ are in general arbitrary functions of Q_g, Q_u^2, and ρ^2. We are going to discuss a different basis for the discrete-state subspace in the next section, thus for clarity, we label the matrix rows and columns by the corresponding discrete states in Eq. (17) and in similar expressions that will follow.

The continuum coupling matrix V_ϵ depends not only on the vibrational coordinates but also on electron energy ϵ. However, the energy dependence does not change the symmetry properties and we can derive the V_ϵ elements in the same way as for U. We obtain

$$V_\epsilon = \begin{array}{c} \\ \Pi_+ \\ \Sigma \\ \Pi_- \end{array} \begin{array}{c} \begin{array}{cccc} s & p_z & p_+ & p_- \end{array} \\ \begin{pmatrix} v_{\Pi s}Q_- & v_{\Pi z}Q_-Q_u & v_{\Pi p} & w_{\Pi p}Q_-^2 \\ v_{\Sigma s} & v_{\Sigma z}Q_u & v_{\Sigma p}Q_+ & v_{\Sigma p}Q_- \\ v_{\Pi s}Q_+ & v_{\Pi z}Q_+Q_u & w_{\Pi p}Q_+^2 & v_{\Pi p} \end{pmatrix} \end{array} \tag{18}$$

where $v_{\Pi s}$, $v_{\Sigma s}$, $v_{\Pi z}$, $v_{\Sigma z}$, $v_{\Pi p}$, $v_{\Sigma p}$, and $w_{\Pi p}$ are again arbitrary functions of totally symmetric coordinates Q_g, Q_u^2, ρ^2 and of the energy ϵ.

The nonlocal potential matrix $F(\epsilon)$ can be obtained directly from Eq. (6). Note that when the E-H_0 operator is substituted for the argument of $F(\epsilon)$, a special attention has to be paid to the evaluation of the operator since the normal coordinates do not commute with H_0. We return to this problem in Sec. VI but for the discussion here and in the next section it is sufficient to consider only $F(\epsilon)$ with ϵ being a positive real number (electron energy). This level-shift potential matrix $F(\epsilon)$ enters the description of the electron scattering from the molecule with fixed positions of nuclei. Now, we can split the integral in Eq. (6) into Hermitian and anti-Hermitian components using the well-known formula $(x+i\eta)^{-1} = \text{v.p.}\, x^{-1} - i\pi\delta(x)$ from theory of distributions, where v.p. is the Cauchy principal value and $\delta(x)$ is the Dirac δ distribution, and we get

$$F_{dd'}(\epsilon) = \Delta_{dd'}(\epsilon) - (i/2)\Gamma_{dd'}(\epsilon), \tag{19a}$$

$$\Gamma_{dd'}(\epsilon) = 2\pi \sum_\mu V_{d\epsilon}^\mu V_{d'\epsilon}^{\mu *}, \tag{19b}$$

$$\Delta_{dd'}(\epsilon) = \frac{\text{v.p.}}{2\pi} \int dx \frac{\Gamma_{dd'}(x)}{\epsilon - x}. \tag{19c}$$

Then the nonlocal matrix F is as follows:

$$F(\epsilon) = \begin{array}{c} \\ \Pi_+ \\ \Sigma \\ \Pi_- \end{array} \begin{array}{c} \begin{array}{ccc} \Pi_+ & \Sigma & \Pi_- \end{array} \\ \begin{pmatrix} F_\Pi(\epsilon) & f_{\Sigma\Pi}(\epsilon)Q_- & f_\Pi(\epsilon)Q_-^2 \\ f_{\Sigma\Pi}(\epsilon)Q_+ & F_\Sigma(\epsilon) & f_{\Sigma\Pi}(\epsilon)Q_- \\ f_\Pi(\epsilon)Q_+^2 & f_{\Sigma\Pi}(\epsilon)Q_+ & F_\Pi(\epsilon) \end{pmatrix} \end{array}, \tag{20a}$$

where imaginary parts multiplied by -2 (the widths) of the F_Π, F_Σ, $f_{\Sigma\Pi}$, and f_Π terms are given from Eq. (19b) by

$$\Gamma_\Pi = 2\pi\left(v_{\Pi s}^2\rho^2 + v_{\Pi z}^2\rho^2 Q_u^2 + v_{\Pi p}^2 + w_{\Pi p}^2\rho^4\right), \tag{20b}$$

$$\Gamma_\Sigma = 2\pi\left(v_{\Sigma s}^2 + v_{\Sigma z}^2 Q_u^2 + 2v_{\Sigma p}^2\rho^2\right), \tag{20c}$$

$$\gamma_{\Sigma\Pi} = 2\pi\left[v_{\Sigma s}v_{\Pi s} + v_{\Sigma z}v_{\Pi z}Q_u^2 + v_{\Sigma p}(v_{\Pi p} + w_{\Pi p}\rho^2)\right], \tag{20d}$$

$$\gamma_\Pi = 2\pi\left(v_{\Pi s}^2 + v_{\Pi z}^2 Q_u^2 + 2v_{\Pi p}w_{\Pi p}\right), \tag{20e}$$

and real parts are given by the Hilbert transform Eq. (19c). In formulas above we for simplicity assumed that functions $v_{d\mu}$, $w_{\Pi p}$ are real.

Before we continue to the fixed-nuclei approximation and static properties of our model, the derived Hamiltonian deserves a few comments. Potential energy surfaces of the Σ and $\Pi_\pm$ discrete states in the diabatic representation are given by $V_0 + E_\Sigma$ and $V_0 + E_\Pi$, respectively. The discrete states are shifted and broadened by the electronic continuum via the $F_\Sigma(\epsilon)$ and $F_\Pi(\epsilon)$ terms, and in addition, they directly interact with each other via off-diagonal elements of the matrix U and also indirectly through the continuum via off-diagonal elements of $F(\epsilon)$. The mutual interaction of the discrete states vanishes not only at the equilibrium geometry, which is the consequence of the definition of the diabatic basis we work in, but also for any linear geometry because the asymmetric stretching can not change the angular momentum of the electronic states. The ξ and $f_\Pi(\epsilon)$ terms are responsible for the Renner-Teller splitting of the shape resonance upon bending. The λ and $f_{\Sigma\Pi}(\epsilon)$ terms cause the interaction of one Renner-Teller component with the virtual state as discussed by Sommerfeld *et al.* [36]. We also see that the continuum coupling V_ϵ Eq. (18) is consistent with our initial discussion in Sec. IIB3, that is, at the equilibrium the virtual state is coupled only to the s wave and the Π_u resonance to the p_+ and p_- (or equivalently to p_x and p_y) waves (p orbitals perpendicular to the molecular axis). However, when the molecule is bent, the Π states can interact with the s wave through the $v_{\Pi s}$ term, which as we will see is important in understanding of a rather peculiar behavior of the lower Renner-Teller state [8]. A deformation of the geometry in Q_u is necessary for the interaction with the p_z wave. The mentioned effects will become more apparent in the fixed-nuclei approximation discussed in the next section and in the discussion of the constructed model in Sec V.

III. FIXED-NUCLEI PROBLEM

We obtain the fixed-nuclei Hamiltonian H_{FN} by omitting the kinetic-energy operator T_N from Eq. (5)

$$H_{\text{FN}} = V_0\mathbb{1} + U + F(\epsilon), \tag{21}$$

where the argument $\epsilon = E - V_0$ (electron energy) of the level-shift function F is no longer an operator. It is important to discuss the electron scattering and eigenenergies of this operator since they will be compared to *ab initio* data to fix the unknown functions E_d, λ, ξ, $v_{d\mu}$, $w_{\Pi p}$ in the model. While the whole vibronic dynamics of our problem respects the full $D_{\infty h}$ symmetry, the symmetry of the fixed-nuclei problem is lowered by deformations of the geometry. The full symmetry is preserved for deformations by pure symmetric stretch $\vec{q} = (Q_g, 0, 0, 0)$. The addition of the asymmetric stretch $\vec{q} = (Q_g, Q_u, 0, 0)$ removes the symmetry plane perpendicular to the molecular z axis and reduces the symmetry to $C_{\infty v}$, while pure bending deformations $\vec{q} = (Q_g, 0, Q_x, Q_y)$ remove the rotational axis and restricts the symmetry to C_{2v}. The molecule deformed in all directions $\vec{q} = (Q_g, Q_u, Q_x, Q_y)$ still has one nontrivial symmetry element (reflection through the molecular plane), i.e., C_s symmetry group. Depending on the geometry the matrix of the fixed-nuclei Hamiltonian Eq. (21) changes its form. As discussed above the matrix is diagonal in the linear $D_{\infty h}$ and $C_{\infty v}$ cases. The structure of the matrix is not completely general even if the molecule is bent. To see this we have to transform the discrete states to obtain a symmetry-adapted basis, which is the same for both the C_{2v} and C_s cases.

A. Transformation to symmetry-adapted basis for deformed geometries

In bent geometries the molecular plane is given by the z axis and the line pointing in the direction of the bending vector $(Q_x, Q_y, 0) \sim (\cos\varphi, \sin\varphi, 0)$. The symmetry-adapted components $\Pi_{||}$ and $\Pi_\perp$ of the $^2\Pi_u$ resonance are obtained by rotating the Cartesian components Π_x, Π_y around the z axis by angle φ:

$$\Pi_{||} = \cos\varphi\,\Pi_x + \sin\varphi\,\Pi_y, \tag{22a}$$

$$\Pi_\perp = -\sin\varphi\,\Pi_x + \cos\varphi\,\Pi_y. \tag{22b}$$

By expressing $\Pi_{||}$ and $\Pi_\perp$ in terms of $\Pi_\pm$, we get

$$\Pi_{||} = (e^{-i\varphi}\Pi_+ + e^{i\varphi}\Pi_-)/\sqrt{2}, \tag{23a}$$

$$\Pi_\perp = (e^{-i\varphi}\Pi_+ - e^{i\varphi}\Pi_-)/\sqrt{2}. \tag{23b}$$

Similarly, $(e^{-i\varphi}|\epsilon p_+\rangle \pm e^{i\varphi}|\epsilon p_-\rangle)/\sqrt{2}$ give the continuum electron partial waves $|\epsilon p_{||}\rangle$ and $|\epsilon p_\perp\rangle$ adapted to the C_{2v} and C_s symmetries.

When $Q_u = 0$, the in-plane component $\Pi_{||}$ transforms according to the same A_1 representation of the C_{2v} group as the Σ virtual state. On the other hand, the $\Pi_\perp$ state, which is perpendicular to the molecular plane, transforms according to the B_1 representation. Using these new basis states the Hamiltonian $H_{\rm FN}$ Eq. (21) splits into two blocks. A 2×2 block that consists of the Σ and $\Pi_{||}$ states and a 1×1 block for the $\Pi_\perp$ state. The same structure is obtained in the general C_s case. The Σ and $\Pi_{||}$ states transform according to the same A' representation and lead to a 2×2 block in $H_{\rm FN}$, while $\Pi_\perp$ transforms according to the A'' representation giving a 1×1 block. We performed all *ab initio* calculations discussed later in the C_s group; therefore, we use the nomenclature of the C_s group for the decoupled problems even in the C_{2v} case. The same reasoning can be applied to the 3×4 discrete-state-continuum coupling matrix V_ϵ. It splits into a 1×1 component $V_\epsilon^{A''}$ that couples the $\Pi_\perp$ state to the $p_\perp$ partial wave and a 2×3 block $V_\epsilon^{A'}$ that couples the Σ, $\Pi_{||}$ discrete states to the s, p_z, and $p_{||}$ partial waves.

For the A'' block describing the upper Renner-Teller component we have

$$H_{A''} = V_0 + U_{A''} + F_{A''}(\epsilon) \tag{24a}$$

with

$$U_{A''} = E_\Pi - \xi\rho^2, \tag{24b}$$

$$F_{A''}(\epsilon) = F_\Pi(\epsilon) - f_\Pi(\epsilon)\rho^2. \tag{24c}$$

Alternatively, we can calculate the nonlocal potential $F_{A''}(\epsilon)$ using Eq. (19) with the coupling amplitude

$$V_\epsilon^{A''} = v_{\Pi p} - w_{\Pi p}\rho^2. \tag{25}$$

For the A' problem comprising of the virtual state interacting with the lower Renner-Teller component the Hamiltonian reads

$$H_{A'} = V_0\mathbb{1}_2 + U_{A'} + F_{A'}(\epsilon), \tag{26a}$$

where $\mathbb{1}_2$ is the 2×2 unit matrix and

$$U_{A'} = \begin{array}{c} \\ \Sigma \\ \Pi_{||} \end{array} \begin{array}{c} \begin{array}{cc} \Sigma & \Pi_{||} \end{array} \\ \begin{pmatrix} E_\Sigma & \sqrt{2}\lambda\rho \\ \sqrt{2}\lambda\rho & E_\Pi + \xi\rho^2 \end{pmatrix} \end{array}, \tag{26b}$$

$$F_{A'}(\epsilon) = \begin{array}{c} \\ \Sigma \\ \Pi_{||} \end{array} \begin{array}{c} \begin{array}{cc} \Sigma & \Pi_{||} \end{array} \\ \begin{pmatrix} F_\Sigma(\epsilon) & \sqrt{2}f_{\Sigma\Pi}(\epsilon)\rho \\ \sqrt{2}f_{\Sigma\Pi}(\epsilon)\rho & F_\Pi(\epsilon) + f_\Pi(\epsilon)\rho^2 \end{pmatrix} \end{array}. \tag{26c}$$

In this case, the coupling amplitudes are given by

$$V_\epsilon^{A'} = \begin{array}{c} \\ \Sigma \\ \Pi_{||} \end{array} \begin{array}{c} \begin{array}{ccc} s & p_z & p_{||} \end{array} \\ \begin{pmatrix} v_{\Sigma s} & v_{\Sigma z}Q_u & \sqrt{2}v_{\Sigma p}\rho \\ \sqrt{2}v_{\Pi s}\rho & \sqrt{2}v_{\Pi z}\rho\,Q_u & v_{\Pi p} + w_{\Pi p}\rho^2 \end{pmatrix} \end{array}. \tag{27}$$

The results of this section are important for the understanding of a very different behavior of the two Renner-Teller components upon bending of the CO_2 molecule [9]. Let us repeat that the originally degenerate $^2\Pi_u$ resonance splits into $^2A_1$ and $^2B_1$ states (in the nomenclature of the C_{2v} group) as the molecule bends, which are described within our model by the diabatic discrete states $\Pi_{||}$ and $\Pi_\perp$, respectively. The $^2A_1$ state ($\Pi_{||}$) is totally symmetric which has two consequences. First, it couples to the electronic s-wave continuum through the $v_{\Pi s}$ term in the nonlocal potential $F_\Pi(\epsilon) + f_\Pi(\epsilon)\rho^2$; see Eqs. (26c), (20b), and (20e). Second, it can also interact with the virtual state Σ either directly through λ [see Eq. (26b)] or indirectly through the electronic continuum via the $f_{\Sigma\Pi}(\epsilon)$ nonlocal potential [see Eqs. (26c) and (20d)]. On the other hand, the $^2B_1$ ($\Pi_\perp$) state is not totally symmetric, and thus, it interacts only with the $p_\perp$ continuum in the nonlocal potential $F_\Pi(\epsilon) - f_\Pi(\epsilon)\rho^2$; see Eqs. (24c), (20b). and (20e). The low-energy dependence of the resonance width for s and p waves is fundamentally different [46] but we return to this problem in Sec. V.

In the end, we should emphasize that the splitting of the Hamiltonian into the 1×1 and 2×2 blocks occurs only in the fixed-nuclei limit. In the vibronic dynamics the change of the symmetry of the electronic states is compensated by the respective change of the symmetry of the vibrational wave function. The dynamics is truly a three-state problem. Similarly, the fixed-nuclei problem depends only on ρ and not on φ, which is hidden in the basis definition, but the dynamics takes place in the full four-dimensional vibrational space.

B. Eigenphase sums

The fixed-nuclei eigenphase sums for each irreducible representation of the symmetry group are decomposed to background and discrete-state (resonant) contributions

$$\delta(\epsilon) = \delta_{\rm bg}(\epsilon) + \delta_{\rm disc}(\epsilon). \tag{28}$$

The background is assumed to be a slowly varying function in both electron energy and nuclear coordinates.

The discrete-state term in the case of one discrete state, as we have in the A'' symmetry, is given by the generalized Breit-Wigner formula [41]

$$\delta^\mu_{\rm disc}(\epsilon) = -\arctan\left(\frac{\Gamma_\mu(\epsilon)/2}{\epsilon - U_\mu - \Delta_\mu(\epsilon)}\right) \tag{29a}$$

with

$$\Delta_\mu(\epsilon) = \mathrm{Re}[F_\mu(\epsilon)], \tag{29b}$$

$$\Gamma_\mu(\epsilon) = -2\ \mathrm{Im}[F_\mu(\epsilon)], \tag{29c}$$

where for the irreducible representation $\mu = A''$ the $U_{A''}$ and $F_{A''}$ terms are given by Eqs. (24b) and (24c). The same formula can be used for linear geometries (both $D_{\infty h}$ and $C_{\infty v}$ cases) where the operator H_{FN} consists only of the diagonal 1×1 blocks corresponding to Σ_g^+ and Π_u irreducible representations. In these cases we substitute $U_\mu = E_\Sigma$ and $F_\mu = F_\Sigma$ for $\mu = \Sigma_g^+$ and $U_\mu = E_\Pi$ and $F_\mu = F_\Pi$ for $\mu = \Pi_u$; see Eqs. (17) and (20).

In the case of the A' symmetry, there are two nontrivial discrete-state eigenphases. Their sum $\delta^{A'}_{\mathrm{disc}}$ can be computed using the following formula derived in Appendix B:

$$\exp\left[2i\delta^{A'}_{\mathrm{disc}}(\epsilon)\right] = \frac{(\epsilon - a^*)(\epsilon - b^*) - c^{2*}}{(\epsilon - a)(\epsilon - b) - c^2}, \tag{30}$$

where $a = \langle\Sigma|U_{A'} + F_{A'}(\epsilon)|\Sigma\rangle$, $b = \langle\Pi_{||}|U_{A'} + F_{A'}(\epsilon)|\Pi_{||}\rangle$, $c = \langle\Sigma|U_{A'} + F_{A'}(\epsilon)|\Pi_{||}\rangle$.

C. Adiabatic potential energy surfaces

Up to this point we have worked in the diabatic representation. To obtain adiabatic potential energy surfaces we need to diagonalize the fixed-nuclei Hamiltonian H_{FN} Eq. (21). We have already partially diagonalized H_{FN} by transforming it to the symmetry-adapted basis, and thus, the adiabatic surface of the A'' state is directly given by Eq. (24). However, this quantity still parametrically depends on the electron energy ϵ, which has to be replaced by a function in the vibrational coordinates $\epsilon_{\mathrm{disc}}(\vec{q})$. For a narrow resonance, the position of the anionic state can be determined from K-matrix poles [41,47]; however, as far as broad resonances or virtual states are concerned, the position should be defined via S-matrix poles [41], that is, by finding $\epsilon_{\mathrm{disc}} = E_R - (i/2)\Gamma_R$ as a complex self-consistent solution of

$$\epsilon_{\mathrm{disc}} - U_\mu - \Delta_\mu(\epsilon_{\mathrm{disc}}) + (i/2)\Gamma_\mu(\epsilon_{\mathrm{disc}}) = 0 \tag{31}$$

for each geometry. Then the adiabatic surface is

$$V^\mu_{\mathrm{adiab}} = V_0 + E_R - (i/2)\Gamma_R. \tag{32}$$

Not only for the A'' problem but also in linear geometries we can use the approach just described. In the case of the A' adiabatic surfaces, we have to first diagonalize the 2×2 Hamiltonian $H_{A'}$ Eq. (26). Its eigenvalues are

$$V_\pm(\epsilon) = V_0 + [\tilde{E}_\Sigma(\epsilon) + \tilde{E}_\Pi(\epsilon)]/2 \pm (1/2)\sqrt{[\tilde{E}_\Sigma(\epsilon) - \tilde{E}_\Pi(\epsilon)]^2 + 4\tilde{\lambda}(\epsilon)^2} \tag{33a}$$

with

$$\tilde{E}_\Sigma(\epsilon) = E_\Sigma + F_\Sigma(\epsilon), \tag{33b}$$

$$\tilde{E}_\Pi(\epsilon) = E_\Pi + F_\Pi(\epsilon) + [\xi + f_\Pi(\epsilon)]\rho^2, \tag{33c}$$

$$\tilde{\lambda}(\epsilon) = \sqrt{2}[\lambda + f_{\Sigma\Pi}(\epsilon)]\rho. \tag{33d}$$

Note that $\tilde{E}_\Sigma$, $\tilde{E}_\Pi$, and $\tilde{\lambda}$ defined above are identical with the constants a, b, and c in Eq. (30). Complex solutions ϵ of $V_\pm(\epsilon) = \epsilon$ give the position of S-matrix poles since they correspond to zeros of the denominator of Eq. (30) in the complex plane.

Locating the S-matrix poles requires to analytically continue the nonlocal potential for complex-valued momenta; see Appendix B of Berman *et al.* [48]. To solve the implicit equations we used Python package CXROOTS [49] that implements methods for finding roots of complex analytical functions described by Kravanja and Barel [50]. The calculation can be simplified when we are interested in only the position of the bound anionic states. Then the imaginary parts in formulas above vanish and we can solve the equations for real (and negative) values of ϵ_{disc} by the bisection method.

IV. MODEL CONSTRUCTION FROM *AB INITIO* DATA

In this section, we determine the model parameters from *ab initio* data. Up to now, we have considered the functions that define the matrix elements of the effective Hamiltonian Eq. (5) to be arbitrary functions of totally symmetric combinations of the normal coordinates. Because computational demands of solving the four-dimensional and nonlocal vibronic dynamics are high, we had to make several simplifications which influenced the parametrization of the model functions. As we discuss in Sec. VI, by expressing the vibrational part of the anionic wave function in a suitable basis, we can rewrite the Schrödinger equation as a system of linear equations. If the Hamiltonian is represented by a sparse matrix, then the linear system can be effectively solved by iterative methods based on Krylov subspaces. By limiting the description of the neutral molecule only to the harmonic approximation, we can effectively evaluate the nonlocal potential $F(E - H_0)$ in a four-dimensional oscillator basis. Note that the evaluation of $F(E - H_0)$ is the most time-consuming step of the calculation. In addition, by restricting the model functions to low-order polynomials in the vibrational coordinates, the Hamiltonian matrix is sparse in the oscillator basis.

The harmonic approximation for the neutral molecule is rather limiting. First, it does not allow for the description of the Fermi resonance which couples nearly degenerate vibrational states of CO_2 [45]. Second, we will see that it is not sufficient for a good quantitative description of the potentials in symmetric stretching. Therefore, our goal is to study qualitative features of the multidimensional and nonlocal vibronic dynamics of the e+CO_2 system. We start the model construction by discussing our *ab initio* calculations.

A. *Ab initio* data

With the above mentioned goal of our work in mind, we approximated the ground electronic state of CO_2 only within the Hartree-Fock approximation with the cc-pVTZ basis [51]. This target description was used as a starting point for fixed-nuclei scattering calculations which were performed using the R-matrix method [52] implemented in the UKRmol+ suite of codes [53]. As a scattering model we chose a static-exchange plus polarization (SEP) model [52] in which one of target valence electrons and an incoming electron are allowed to occupy several lowest unoccupied orbitals above the highest-occupied molecular orbital which are called virtual orbitals. The number of used virtual orbitals in the final scattering SEP

calculations was chosen in such a way to reproduce approximately the autodetachment region for symmetric stretch as was obtained by Sommerfeld *et al.* [36].

We tried several models with 10–20 virtual orbitals and optimal results for symmetric stretch were obtained for 18 virtual orbitals. The L^2 configurations [52] used in the final SEP model were of the type

$$(\text{core})^6(\text{valence})^{16}(\text{virtual})^1 \tag{34}$$

and

$$(\text{core})^6(\text{valence})^{15}(\text{virtual})^2. \tag{35}$$

Thus, three lowest (core) molecular orbitals were kept frozen and one of valence electrons from other eight occupied orbitals was allowed to excite to one of 18 virtual orbitals to take into account polarization of the target. The R-matrix sphere radius was set to 13 bohrs which was sufficient for the SEP scattering calculations (all used target orbitals were well-contained in the R-matrix sphere). The same model was also used to calculated energies of the anionic states in the regions where these states are bound to have additional information for construction of the model for the nuclear dynamics. We performed the above described fixed-nuclei calculations for more than 2000 nuclear configurations around the equilibrium geometry of CO_2 varying all three normal coordinates.

B. Parametrization of the model functions

Our model is determined if we know twelve functions V_0, E_d, λ, ξ, $v_{d\mu}$, $w_{\Pi p}$ of totally symmetric combinations of the normal coordinates, i.e., the potential energy surface of the neutral molecule and the functions entering the matrices U and V_ϵ. Considering the simplifications discussed at the beginning of this section, we use

$$V_0 = \tfrac{1}{2}\omega_g Q_g^2 + \tfrac{1}{2}\omega_b \rho^2 + \tfrac{1}{2}\omega_u Q_u^2, \tag{36}$$

where ω_g, ω_b, and ω_u are vibrational angular frequencies of symmetric stretching, bending and asymmetric stretching of CO_2, respectively. We specify their numerical values based on our quantum chemical calculations later. The other model functions were chosen as low-order polynomials in Q_g, Q_u^2, and ρ^2 and the number of terms in each polynomial was carefully chosen to get a reasonable agreement with the *ab initio* data. We explicitly show only the expansion of the functions into Q_u^2 and ρ^2. The remaining parameters are polynomials in Q_g up to the fourth order.

The parameters E_Π and E_Σ on the diagonal of the matrix U [see Eq. (17)] are the most important. They describe the energy of the discrete states relative to the threshold V_0. Thus, we included more terms than in other cases, and we have

$$E_\Pi = E_\Pi^0 + E_\Pi^{2b}\rho^2 + E_\Pi^{2u}Q_u^2 + E_\Pi^{4b}\rho^4, \tag{37}$$

$$E_\Sigma = E_\Sigma^0 + E_\Sigma^{2b}\rho^2 + E_\Sigma^{2u}Q_u^2 + E_\Sigma^{4b}\rho^4 + E_\Sigma^{4u}Q_u^4 + E_\Sigma^{4bu}\rho^2 Q_u^2. \tag{38}$$

In the case of the Renner-Teller coupling ξ, which is multiplied by $Q_\pm^2$ in the matrix U, we added one extra term in bending

$$\xi = g + \kappa\rho^2. \tag{39}$$

The $\Sigma\Pi$ coupling λ is assumed to be only a polynomial in Q_g.

In the case of the continuum coupling V_ϵ given by Eq. (18), we parametrized the coupling between the $\Pi_\pm$ discrete states and the $p_\pm$ partial waves in the following way:

$$v_{\Pi p} = v_{\Pi p}^0 + v_{\Pi p}^{2b}\rho^2 + v_{\Pi p}^{2u}Q_u^2 \tag{40}$$

and similarly for the coupling of the Σ discrete state to the s wave:

$$v_{\Sigma s} = v_{\Sigma s}^0 + v_{\Sigma s}^{2b}\rho^2 + v_{\Sigma s}^{2u}Q_u^2. \tag{41}$$

We can expect that these terms are going to be the most important since only these couplings are nonzero at the equilibrium geometry and the incoming electron is captured to the CO_2 molecule in its ground vibrational state. For the coupling of the $\Pi_\pm$ states to the s wave, we used

$$v_{\Pi s} = v_{\Pi s}^0 + v_{\Pi s}^{2u}Q_u^2. \tag{42}$$

The remaining terms

$$v_{\Sigma z},\ v_{\Sigma p},\ v_{\Pi z}, w_{\Pi p} \tag{43}$$

are assumed to be only polynomials in Q_g.

The continuum coupling terms depend not only on the normal coordinates but primarily on electron energy. Each coefficient in Eqs. (40)–(43) is independently parametrized by the Wigner threshold law [46] multiplied by an exponential cutoff function [41]

$$v(\epsilon) = a(\beta\epsilon)^{(2l+1)/4}e^{-\beta\epsilon}, \tag{44}$$

where $l = 0$ for the s-wave coupling, $l = 1$ for p_z or $p_\pm$ waves, a is a polynomial in Q_g, and β is a constant. Using the parametrization above, we can calculate the integral that appears in the shift operator $\Delta_{dd'}(\epsilon)$ Eq. (19c) in terms of the incomplete Gamma function and confluent hypergeometric function; see Eq. (24) in Ref. [54]. By considering the threshold exponent $(2l+1)/4$ and the β parameter constant, $v(\epsilon)$ is separable in the energy and normal coordinates which simplifies the evaluation of $F(E - H_0)$. However, a constant threshold exponent prevents the description of a geometry-dependent dipole moment [55]. The CO_2 molecule does not possess any dipole moment in its equilibrium geometry but it acquires one in bent or asymmetrically stretched geometries. This deficiency of our model may be important especially in the threshold region.

Finally, we used the following parametrization of the background eigenphase sums

$$\delta_{\text{bg}}^{A''}(\epsilon) = a_{\text{bg}}\epsilon + b_{\text{bg}} + b_{\text{bg}}^{2b}\rho^2 + b_{\text{bg}}^{2u}Q_u^2, \tag{45}$$

$$\delta_{\text{bg}}^{A'}(\epsilon) = \left(c_{\text{bg}} + c_{\text{bg}}^{1b}\rho + c_{\text{bg}}^{2u}Q_u^2\right)\epsilon + d_{\text{bg}} + d_{\text{bg}}^{1b}\rho + d_{\text{bg}}^{2u}Q_u^2 + d_{\text{bg}}^{3bu}\rho\, Q_u^2 \tag{46}$$

in fitting the *ab initio* fixed nuclei data.

C. Fitting procedure

In the case of the neutral potential V_0, our original idea was to use experimental values of the vibrational frequencies, which are [56] $\omega_b^{\text{exp}} = 83.3\,\text{meV}$, $\omega_g^{\text{exp}} = 167.5\,\text{meV}$, and $\omega_u^{\text{exp}} = 297.1\,\text{meV}$. However, we found out that the description of the neutral molecule within our R-matrix model

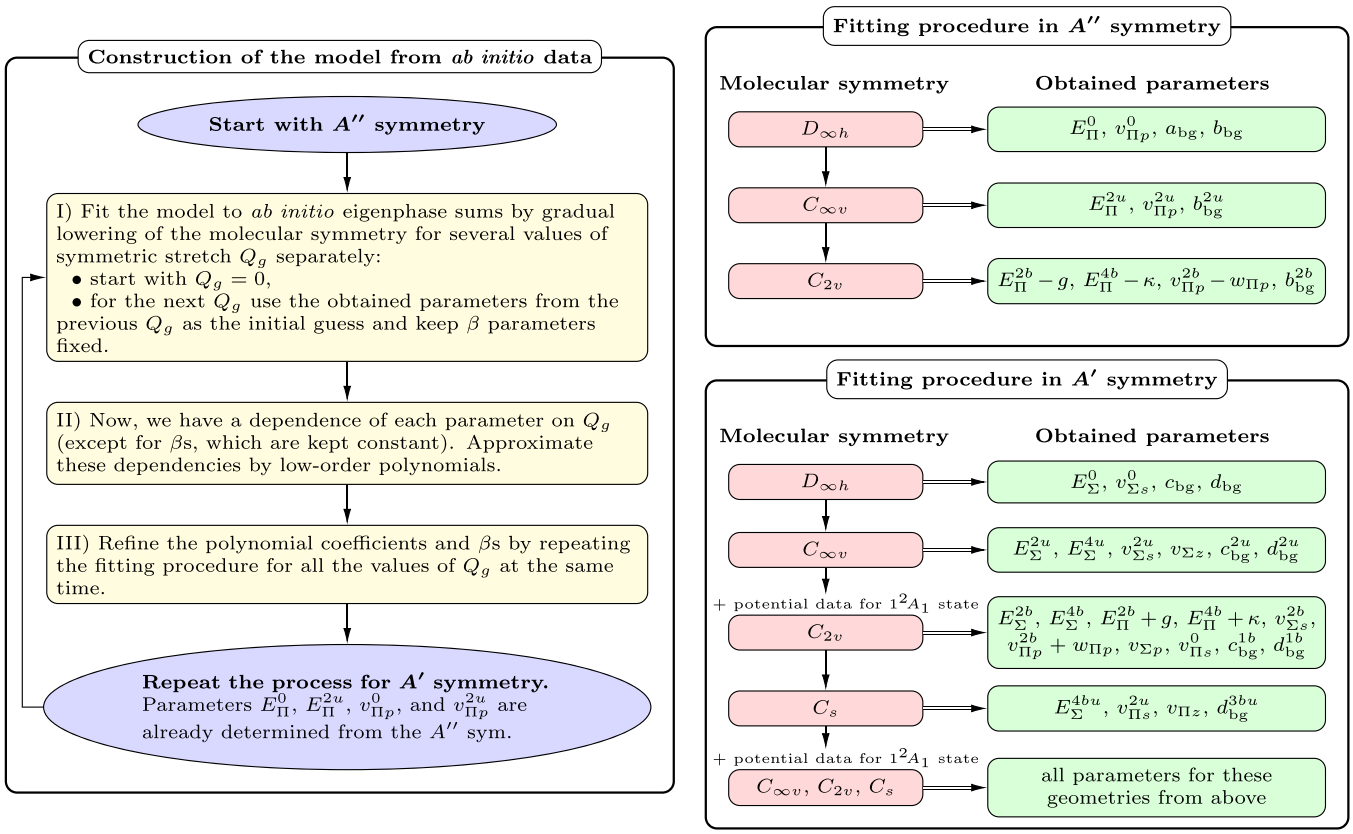

FIG. 1. Illustration of the construction of the model from *ab initio* R-matrix eigenphase sums and potential energies.

is not ideal in comparison with the spectroscopic data. In order to have the consistent description of the potentials and eigenphase sums, we decided to determine the vibrational frequencies by fitting the quadratic form to the potential energies of the CO_2 target obtained within the R-matrix scattering calculations; see Sec. IV A. The fit of the data close to the equilibrium geometry provided $\omega_b = 110\,\text{meV}$ and $\omega_u = 308\,\text{meV}$. The agreement on the asymmetric stretching is reasonable but the bending frequency in our model is about 30% higher than the experimental value. In the case of the symmetric stretching we obtained 196 meV from the fit, but we decided to use $\omega_g = 2\,\omega_b = 220\,\text{meV}$ instead to preserve the $\omega_b^{\rm exp}/\omega_g^{\rm exp}$ ratio important for the Fermi resonance [45].

We determined numerical values of the model functions E_d, λ, ξ, $v_{d\mu}$, $w_{\Pi p}$ by a least-squares fit to the *ab initio* eigenphase sums and potential energy surfaces for electron energies up to about 5 eV relative to the minimum of the neutral potential. Although the number of parameters is large, the splitting into the A' and A'' symmetries and gradual lowering of the molecular symmetry make the fitting feasible because only subsets of parameters contribute at different molecular symmetries.

The construction process illustrated in Fig. 1 has three main steps. In step I, we performed separate fits to the R-matrix eigenphase sums in the A'' symmetry for symmetric stretches $S_g \in \{0.0, \pm 0.2, \pm 0.4, 0.6\}$ bohrs. The fitting was divided into the $D_{\infty h}$, $C_{\infty v}$, and C_{2v} symmetries as it is indicated in the top right-hand part of Fig. 1, where the sequence in which the parameters are obtained is also shown. We did not consider C_s geometries in the A'' case since there are no parameters appearing exclusively in this symmetry and the prediction of the model constructed in other symmetries was good enough. For each symmetry we included the eigenphase sums for several geometries at the same time. The A'' results depend on $E^{2b}_\Pi - g$, that is we can not obtain values for the individual terms E^{2b}_Π and g. On the other hand, the A' results depend on their sum; therefore, we can obtain values of E^{2b}_Π and g afterwards. We dealt with E^{4b}_Π, κ, $v^{2b}_{\Pi p}$, and $w_{\Pi p}$ in the same way.

The result of step I is the S_g dependence of the parameters given by series of six values. We approximated them by polynomials up to the fourth order in step II. We performed the fitting procedure from step I once again to improve the polynomial coefficients and the β parameters in step III, but this time we included data for all the values of S_g at the same moment. We did not include the position of the $^2B_1$ state where it is bound since its energy in this region is too high.

We repeated the three steps for the A' symmetry. The fitting procedure is more elaborate (see bottom right-hand part of Fig. 1) because there are two A' states. We included the R-matrix position of the $1\,^2A_1$ bound state in the fitting of the C_{2v} symmetry. We also performed a fit of C_s geometries since there are parameters that appear exclusively for these configurations in this case. The model constructed from these fits did not reproduce the eigenphase sums sufficiently well. To improve the agreement further, we performed one more fit where we varied all parameters that depend either on bending or asymmetric stretch for the $C_{\infty v}$, C_{2v}, and C_s geometries used in the previous fits.

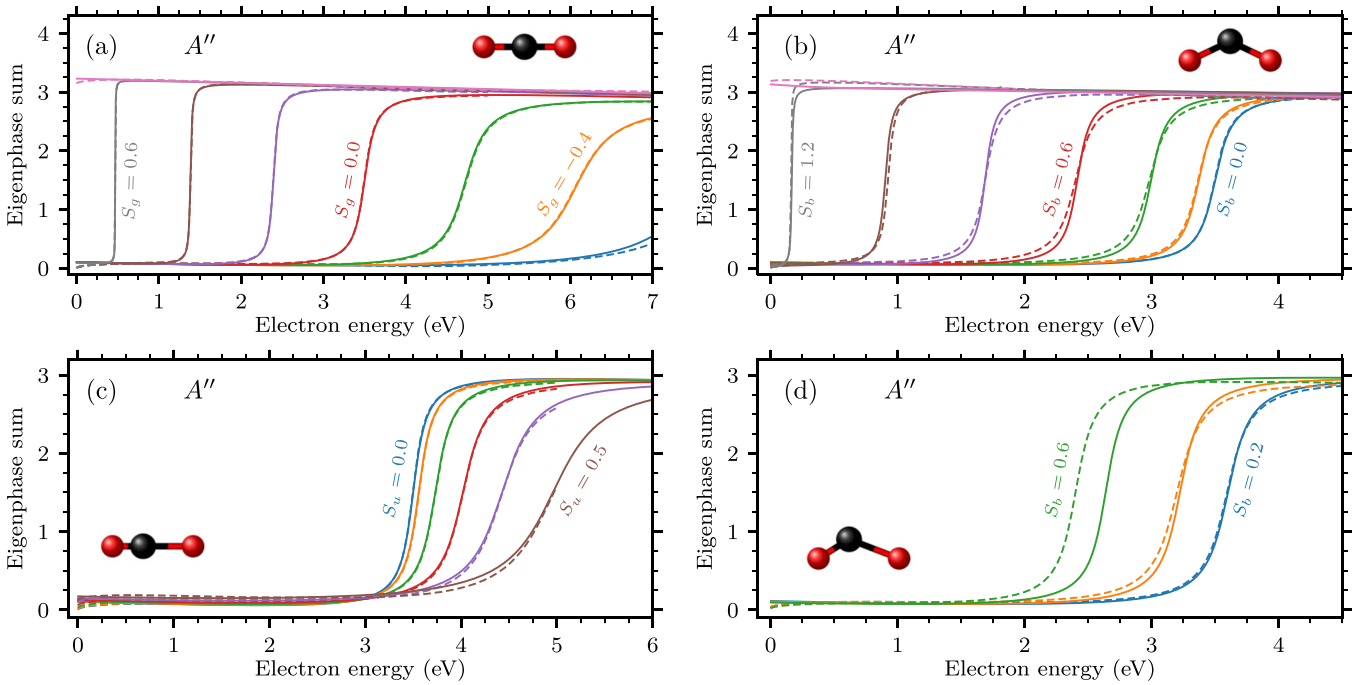

FIG. 2. Eigenphase sums in the A'' symmetry; solid lines, model; dashed lines, R-matrix data. (a) Symmetrically stretched geometries for $S_b = 0$, $S_u = 0$, and $S_g = -0.6$, -0.4, -0.2, 0.0, 0.2, 0.4, 0.6, and 0.8 bohrs (from right to left). (b) Bent geometries for $S_g = 0$, $S_u = 0$, and $S_b = 0.0$, 0.2, 0.4, 0.6, 0.8, 1.0, and 1.2 bohrs (from right to left). (c) Asymmetrically stretched geometries for $S_g = 0$, $S_b = 0$, and $S_u = 0.0$, 0.1, 0.2, 0.3, 0.4, and 0.5 bohrs (from left to right). (d) Bent and asymmetrically stretched geometries for $S_g = 0$, $S_u = 0.2$, and $S_b = 0.2$, 0.4, and 0.6 bohr (from right to left).

We list the resulting values of all parameters in Appendix C. A comparison of the *ab initio* eigenphase sums of the A'' symmetry with their reproduction by our model is shown in Fig. 2 for a selected set of geometries. The moderately wide resonance corresponds to the $^2A''$ Renner-Teller component of the $^2\Pi_u$ shape resonance ($^2B_1$ in the C_{2v} nomenclature). It moves closer to the threshold and its width decreases as the molecule symmetrically stretches and it eventually becomes bound; see Fig. 2(a). Although the eigenphase sums for $S_g = -0.6$ and 0.8 bohrs were not included into the fitting process, the agreement with the R-matrix data is very good even for these geometries. The resonance also becomes bound upon bending; see Fig. 2(b). Note that upon change of S_b, the angle changes simultaneously with the bond length. This does not allow for the direct comparison with eigenphase sums of Morgan [21]. However, our results are in agreement with hers when recalculated for varying only the bending angle. Our model reproduces the resonance position well but there is some disagreement in its width. The width is described by the $v^{2b}_{\Pi p} - w_{\Pi p}$ parameter, which depends on ρ^2. Adding another term of the fourth order in ρ did not significantly improved the agreement and we were reluctant to increase the complexity of the model even more with regard to the feasibility of the dynamics. For asymmetric stretches the resonance moves further from the threshold [see Fig. 2(c)], and finally, Fig. 2(d) shows the data for general, both bent and asymmetrically stretched, geometries. The results shown in Fig. 2(d) are solely predictions of the model since the C_s geometries were not included to the fitting process.

Figure 3 shows the A' model eigenphase sums in comparison with the R-matrix data. The Renner-Teller states are degenerate for symmetrically stretched geometries, thus, the eigenphase sums exhibit the same resonance behavior as in the A'' symmetry; compare Fig. 3(a) with Fig. 2(a). The virtual state manifests itself in the behavior near the threshold and it also becomes bound for S_g between 0.6 and 0.8 bohrs. The data for $S_g = 0.8$ bohrs were not included into the fitting procedure again, but the agreement is still reasonable. A dramatically different behavior of the A' Renner-Teller component in contrast to the A'' component is observed upon bending; see Fig. 3(b). The A' state moves towards the threshold and its width is substantially increased, which agrees with Morgan [21]. For $S_b > 0.35$ bohrs the state becomes so wide that it is not observable in the eigenphases any more. Moreover, the threshold region and the resonance are not separated as for pure symmetric stretches since the states interact with each other.

For asymmetric stretches the model is not able to reproduce the low-energy behavior well; see Fig. 3(c). The CO_2 molecule acquires a dipole moment which becomes supercritical for $S_u > 0.22$ bohrs. As a result, the eigenphase sums logarithmically diverge at the threshold for these geometries [57]. The threshold behavior is controlled by the threshold exponent that becomes geometry dependent [55] and vanishes at the critical value of the dipole moment. Such behavior is not reflected in our model where the threshold exponent is given by the pure s- and p-wave behavior; see Eq. (44). In addition, the fact that the exponential parameters β in Eq. (44) are kept independent of the vibrational coordinates reduces the flexibility of the model as well. We expect that this model limitation will influence the low-energy behavior of the cross sections. The CO_2 molecule also acquires a dipole moment

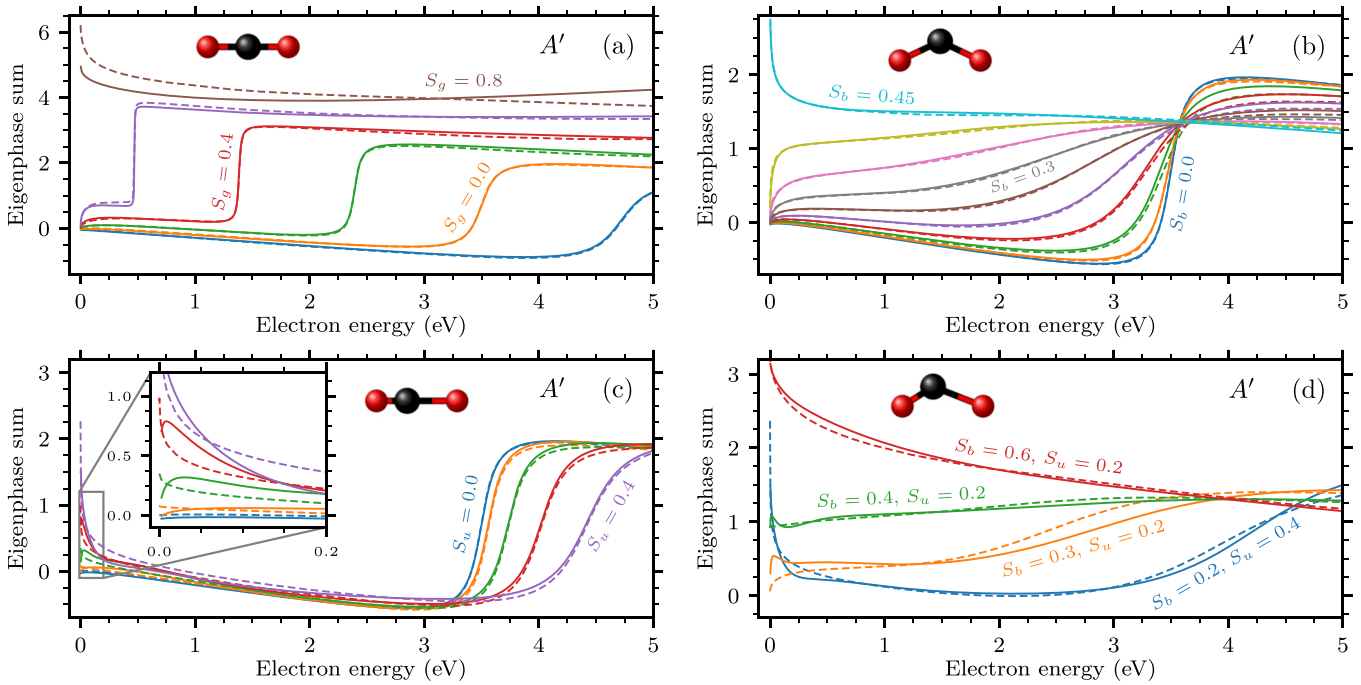

FIG. 3. Eigenphase sums in the A' symmetry; solid lines, model; dashed lines, R-matrix data. (a) Symmetrically stretched geometries for $S_b = 0$, $S_u = 0$, and $S_g = -0.2$, 0.0, 0.2, 0.4, 0.6, and 0.8 bohrs (from right to left). (b) Bent geometries for $S_g = 0$, $S_u = 0$, and for S_b from 0.0 to 0.45 bohrs with step 0.05 bohr (from right to left). (c) Asymmetrically stretched geometries for $S_g = 0$, $S_b = 0$, and $S_u = 0.0$, 0.1, 0.2, 0.3, and 0.4 bohrs (from left to right). The inset shows a detail of the threshold region. (d) Bent and asymmetrically stretched geometries for $S_g = 0$, values of S_b and S_u are in the figure.

upon bending, but it becomes critical for very large deviations ($S_b = 1.0$ bohrs) from the equilibrium geometries. Finally, the agreement for geometries that are simultaneously bent and asymmetrically stretched is reasonable; see Fig. 3(d).

We showed only the comparison of the R-matrix and model eigenphase sums for a relatively small subset of calculated geometries. In total, R-matrix data for about 400 geometries were used to construct the model, which overall reproduces the data well.

V. DISCUSSION OF THE RESULTING MODEL

The fitting process described above is ambiguous in determination of the parameters. Since the model construction involves nonlinear least-squares fits with many parameters, we have no guarantee that the resulting parameters correspond to the global minimum of the least-squares cost function. Furthermore, the cost function itself is sensitive to the exact data set (energy and geometry ranges) included in the fitting procedure and the relative importance of different subsets of data (different symmetries, eigenphase sums versus potentials) is not clearly given. We therefore constructed a second model that reproduces the *ab initio* data with a similar accuracy as the model with the parameters listed in Appendix C. Although some parameters of the second model differ quite considerably (about up to a factor of 5), the dynamics based on these two models lead to similar electron energy-loss spectra which will be discussed in a follow-up to this paper. In what follows we discuss the properties of the first model. The behavior of the second model is qualitatively the same.

A. Adiabatic potentials

Cuts through the model adiabatic potential energy surfaces calculated from the S-matrix poles as described in Sec. III C are shown in Fig. 4. Potential energies V with a nonzero imaginary part $-\Gamma/2$ are plotted as shaded areas between $V \pm \Gamma/2$. There is no resonance width associated with the virtual state since the corresponding S-matrix poles are located on the negative real axis on the unphysical sheet in the energy complex plane [58]. In Fig. 4 we indicate geometries where the anionic states are not bound by dashed lines. The picture in linear geometries is rather simple since the degenerate $^2\Pi_u$ shape resonance and the Σ_g^+ virtual state do not interact with each other. The shape resonance becomes bound first at symmetric stretch $S_g = 0.7$ bohrs, which corresponds to the C–O distance $R_{CO} = 2.55$ bohrs, and the virtual state merges with the neutral potential at $S_g = 0.8$ bohrs ($R_{CO} = 2.6$ bohrs); see Fig. 4(a). In the case of the asymmetric stretching, the shape resonance is in the continuum for all relevant geometries; see Fig. 4(c). The R-matrix calculations do not show that the virtual state should become bound at any asymmetric stretch; however, it becomes very weakly bound for $S_u > 0.37$ bohrs ($R_{CO}^{(1)} < 1.83$ bohrs and $R_{CO}^{(2)} > 2.57$ bohrs) in our model. The disagreement is caused by the absence of the dipole moment induced by deformation of the molecule in our model as discussed in Sec. IV B.

The situation is very interesting upon bending of the molecule; see Fig. 4(b). The upper Renner-Teller component $^2B_1$ is not much affected by the bending, and it becomes bound at $S_b = 1.25$ bohrs ($R_{CO} = 2.53$ bohrs and the O–C–O angle $\angle OCO = 121°$). On the other hand, the lower component

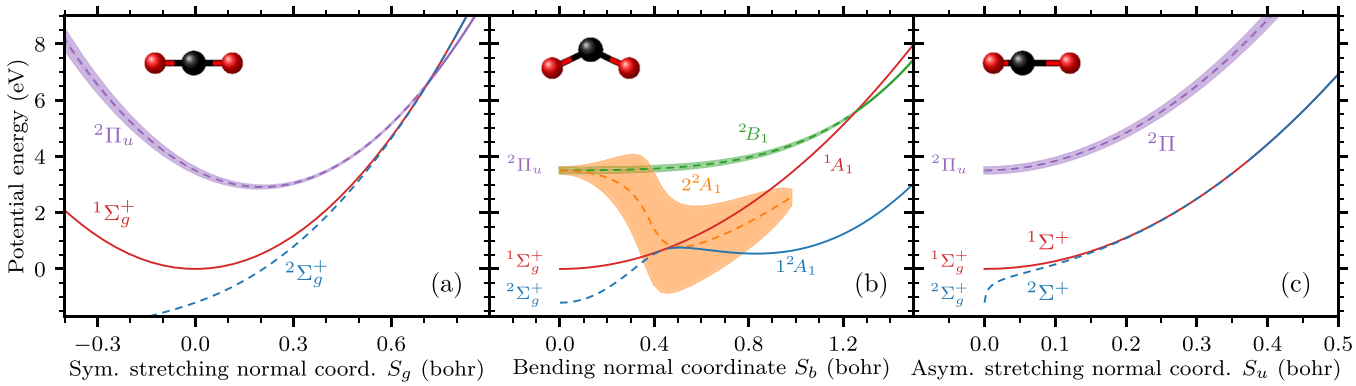

FIG. 4. Adiabatic potential energy curves of CO_2 and CO_2^- within our model; solid lines, geometries where states are bound; dashed lines, geometries where states are not bound. The shaded areas represent the resonance width of the Renner-Teller states. (a) Symmetric stretching geometries S_g, $S_b = 0$, $S_u = 0$. (b) Bending geometries S_b, $S_g = 0$, $S_u = 0$. (c) Asymmetric stretching geometries S_u, $S_g = 0$, $S_b = 0$.

$2\,^2A_1$ quickly moves to the threshold and its width rapidly increases. The virtual state becomes bound at $S_b = 0.45$ bohrs ($R_{CO} = 2.24$ bohrs, $\angle OCO = 157°$) and possesses a minimum at $S_b = 0.83$ bohrs ($R_{CO} = 2.35$ bohrs, $\angle OCO = 139°$), which is in good agreement with Sommerfeld *et al.* [36]. The lower Renner-Teller component gets very close to the virtual state $1\,^2A_1$ and also crosses the neutral curve; however, it does not become bound. This behavior is more easily understandable in terms of the movement of the S-matrix poles shown in Fig. 5. The pole representing the virtual state is located

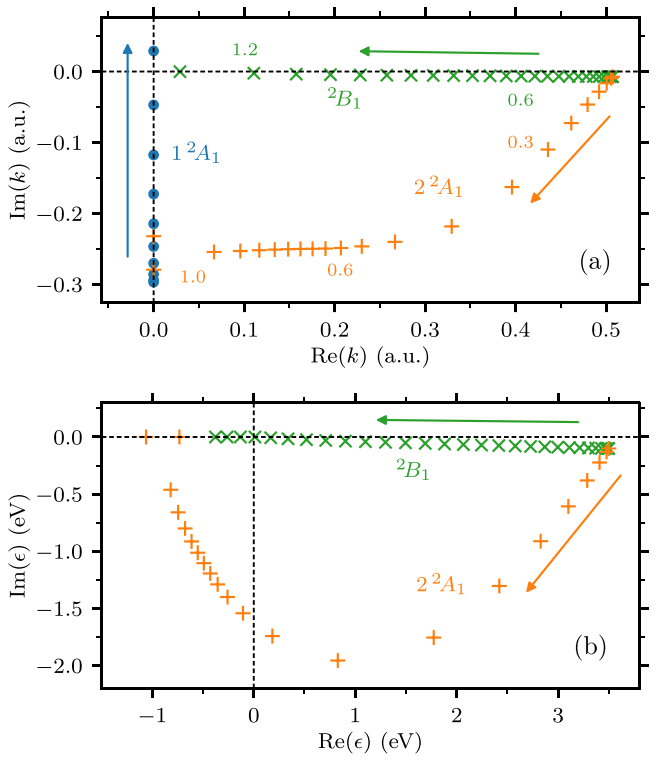

FIG. 5. Movement of S-matrix poles of the CO_2^- states in (a) momentum and (b) energy complex planes upon bending ($S_g = 0$, $S_u = 0$). The bending normal coordinate S_b increases from the equilibrium geometry in the direction of the arrows. Selected geometries S_b are labeled by the numbers. Pluses, $2\,^2A_1$ Renner-Teller state; crosses, $^2B_1$ Renner-Teller state; circles, $1\,^2A_1$ virtual state.

at $k = -0.3i$ a.u. at the equilibrium geometry of CO_2, which quite differs from values $k = -0.16i$ and $-0.2i$ reported by Morisson [19] and Morgan [21], respectively. The pole moves along the imaginary axis up as S_b increases, and it becomes a bound state at $S_b = 0.45$ bohrs. The poles representing the Renner-Teller components coincide at the equilibrium geometry at $k = (0.507 - 0.007i)$ a.u. The $^2B_1$ component moves closer to the origin, and it becomes bound at $S_b = 0.7$ bohrs while the $2\,^2A_1$ component rapidly moves further away from the real axis. It gets on the imaginary axis for geometries $S_b > 1.0$ bohrs where two poles emerge. One of them moves down along the imaginary axis and the other up and becomes bound for $S_b > 1.5$ bohrs. However, the $2\,^2A_1$ state is not controlled well in the fitting procedure for $S_b \gtrsim 0.35$ bohrs because the state is so wide that it does not manifest itself in the eigenphase sums; see Fig. 3(b). Therefore, we expect that the behavior for highly bent configurations is the result of extrapolation of the model and probably is not physically relevant; see below.

When we plot the poles in the energy complex plane [see Fig. 5(b)], the $2\,^2A_1$ poles have a negative real part, which is measured relative to the threshold, for large values of S_b. Thus, the potential energy surface crosses the neutral surface V_0 but it does not become a true bound state. In fact, the state is so far away in the complex plane that it should not probably be called a resonance any more and its position is not well defined. For clarity, we do not show the $1\,^2A_1$ poles in Fig. 5(b). They move on the negative real axis on the unphysical sheet towards the origin where they emerge on the physical sheet.

In reality, the $1\,^2A_1$ state is affected by the dipole moment acquired upon bending [59], which is not included in our model, and the corresponding pole moves along a parabolic trajectory as shown in the R-matrix calculations of Morgan [21]. Nevertheless, the avoided crossing of the $1\,^2A_1$ and $2\,^2A_1$ states within our model is in agreement with findings of Sommerfeld *et al.* [35,36]; see also our discussion in the introduction.

In Fig. 6 we compare our potentials (solid lines) with the *ab initio* model of McCurdy *et al.* [9] (dashed lines), who treated the nuclear dynamics of both the Renner-Teller components upon symmetric stretching and bending in the LCP approximation. In fact, their $2\,^2A_1$ surface was constructed in the earlier work by Rescigno *et al.* [8]. Unfortunately, they do

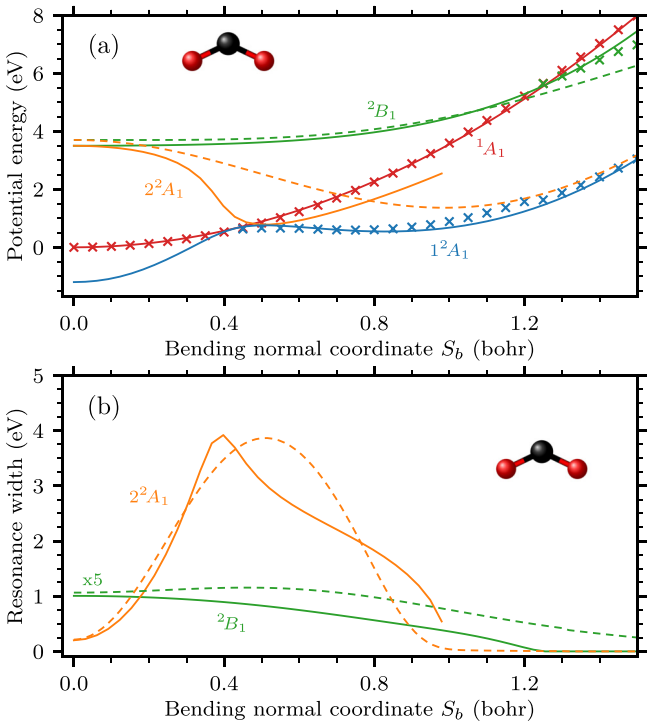

FIG. 6. (a) Real parts and (b) widths of the adiabatic potential energy curves upon bending ($S_g = 0$, $S_u = 0$) for the $1\,^2A_1$ virtual state and $2\,^2A_1$ and $^2B_1$ Renner-Teller components of the $^2\Pi_u$ resonance. Solid lines, our model; dashed lines, model of McCurdy *et al.* [9]; crosses, our R-matrix data for positions of bound states. The $^2B_1$ resonance width in (b) is multiplied by factor 5.

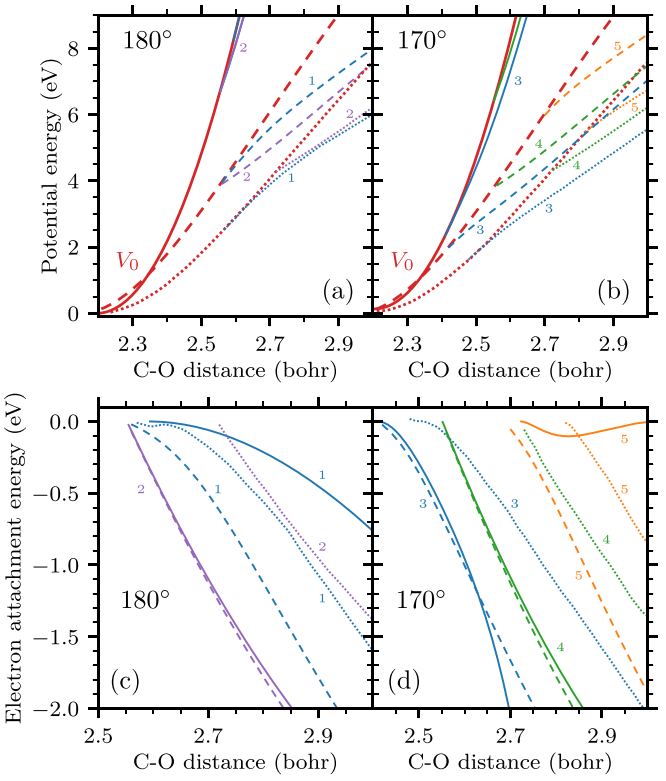

FIG. 7. Harmonic approximation to the neutral CO_2 potential and its influence on the adiabatic potential energy surfaces of CO_2^-; solid lines, our model; dashed lines, our R-matrix data; dotted lines, data of Sommerfeld *et al.* [36]. The neutral potentials are shown by thicker lines and anionic states are labeled by numbers: 1, $^2\Sigma_g^+$; 2, $^2\Pi_u$; 3, $1\,^2A_1$; 4, $^2B_1$; 5, $2\,^2A_1$. Panels (a) and (b) show cuts through the neutral and anionic surfaces for symmetric stretches with fixed O-C-O angles of 180° and 170°, respectively. Panels (c) and (d) show electron attachment energies of the anionic states for the same bond angles as above.

not report their neutral potential, and we suspect that there is an inconsistency in the definition of the bend angle throughout Refs. [8,9], where potential plots state that the data are shown with respect to the bend angle $\theta = \pi - \measuredangle$OCO but then the potential minimum corresponds to $\measuredangle$OCO = 152° which is in a disagreement with other works [30,31,35,36] which place the minimum at 135°–140°. This notable difference is not discussed in Refs. [8,9], and thus, we believe that their data are actually shown with respect to $\theta/2$ since then the minimum is at 134°, and it is consistent with their definition of normal coordinates; see Sec. III in Ref. [8]. We took this into considerations when we plotted their potentials with respect to our bending normal coordinate S_b in Fig. 6. The width of the $^2B_1$ state in our model is somewhat smaller because of our imperfect fit [see Fig. 2(b)], but the position agrees very well. Since the model of McCurdy *et al.* [9] does not include the virtual state, the potential minimum connects to the $^2\Pi_u$ resonance but the $2\,^2A_1$ widths are in a qualitative agreement. The authors of Ref. [8] faced the same difficulties during the construction of the model from *ab initio* data as we did: the $2\,^2A_1$ state gets so wide as CO_2 bends that there are no longer any observable effects in the fixed-nuclei eigenphase sums or cross sections; see Sec. III A of Ref. [8]. They smoothly interpolated results of their fit and energies of the ground state of CO_2^-. In our case the decrease of the width is the result of extrapolation of the model beyond $S_b = 0.4$ bohrs. Although the topology of the anionic surfaces of CO_2^- is interesting, it does not seem to affect the vibrational excitation of CO_2 in the energy region of the $^2\Pi_u$ resonance (2–5 eV). Rescigno *et al.* [8] reported that the cross sections are insensitive to the interpolation of the width at highly bent geometries since the molecular anion CO_2^- is formed by the vertical electron attachment at the equilibrium geometry of CO_2 and with high probability the anion decays before reaching highly bent configurations. Our nonlocal calculations support this conclusion at these energies and we will discuss it more in a follow-up to this paper.

The quantitative description of the potential energy surfaces is limited by the harmonic approximation of the neutral molecule used in order to keep the dynamics feasible. The model reproduces the R-matrix neutral potential in the direction of pure bending very well (see Fig. 6) since we fitted the bending vibrational frequency to these data. There is a similarly good agreement for pure antisymmetric stretches. However, the agreement is rather poor in the symmetric stretching direction. The *ab initio* neutral potential is anharmonic in its shape, and furthermore, we did not use the frequency corresponding to the potential itself but we used the double of the bending frequency in this case; see Sec. IV C.

Figure 7 shows a comparison of the model potentials (solid lines) with our R-matrix data (dashed lines) and with

calculations of Sommerfeld *et al.* [36] (dotted lines). When comparing these three data sets, we observe a similar behavior on the qualitative level but there are notable quantitative differences. The description of the neutral molecule at the Hartree-Fock level within our SEP scattering calculations does not fully describe the electron correlation energy and produces the bending vibrational frequency of CO_2 about 30% larger than the experimental value; see Sec. IV C. We therefore expect that the equation-of-motion coupled-cluster potentials [36] are more accurate. For linear geometries the order of states in the R-matrix calculation is reversed ($^2\Pi_u$ state below $^2\Sigma_g$) compared to Ref. [36], but both the calculations are consistent in this respect when the molecule is bent, i.e., the anion states are bound in the order $1\,^2A_1$, $^2B_1$, $2\,^2A_1$. The harmonic approximation for V_0 causes the vertical discrepancy between the model and the R-matrix potentials but the electron attachment energy (energy difference between anionic and neutral states) agrees well for potential energies up to about 5 eV above the ground vibrational state of CO_2.

B. Role of individual terms in the model

Let us now focus on examining the effect of model parameters on the behavior of the anionic states upon bending. The origin of the $1\,^2A_1$ state potential minimum at nonlinear, i.e., bent geometries (we will use the term *nonlinear minimum* below for short) is related to the square root that appears in the formula for the adiabatic surfaces in Eq. (33) since the discrete-state potentials $V_0 + E_\Sigma$ and $V_0 + E_\Pi$ do not possess any nonlinear minima. The first term in the square root depends on the Renner-Teller coupling through the ξ and $f_\Pi(\epsilon)$ functions and the second on the $\Sigma\Pi$ coupling through λ and $f_{\Sigma\Pi}(\epsilon)$. In principle both coupling mechanisms can lead to the formation of a nonlinear minimum; see also the discussion of Köppel *et al.* [37]. We found that the direct $\Sigma\Pi$ coupling given by λ has a minor effect; see Fig. 8, where dotted lines are calculated from our model but with $\lambda = 0$. The coupling of the $2\,^2A_1$ Renner-Teller state to the s wave represented by the $v_{\Pi s}$ function is responsible not only for the rapid broadening of the resonance width but also for the nonlinear minimum; see dashed lines in Fig. 8, which are calculated with $v_{\Pi s} = 0$. Finally, dot-dashed lines in Fig. 8 show results if we set all parameters related to the virtual state to zero. Even in this case the minimum does not disappear. The direct Renner-Teller term ξ affects the potential curves quite significantly (see Fig. 9), but the nonlinear minimum still exists. On the other hand, the indirect coupling through the $w_{\Pi p}$ functions is rather negligible.

To summarize, the twofold degenerate $^2\Pi_u$ resonance splits into the $2\,^2A_1$ and $^2B_1$ states upon bending of the CO_2 molecule partly due to the Renner-Teller effect but especially because of the coupling of the $2\,^2A_1$ component to the s wave. Because of this coupling the $2\,^2A_1$ state tends to become bound and connect to the nonlinear minimum but the presence of the $1\,^2A_1$ virtual state leads to the avoided crossing of the corresponding potential energy surfaces in the adiabatic representation. Nevertheless, we expect that the character of the adiabatic electronic wave functions changes along the bending coordinate. In other words, there is a diabatic electronic state that connects the $^2\Pi_u$ resonance with the nonlinear minimum.

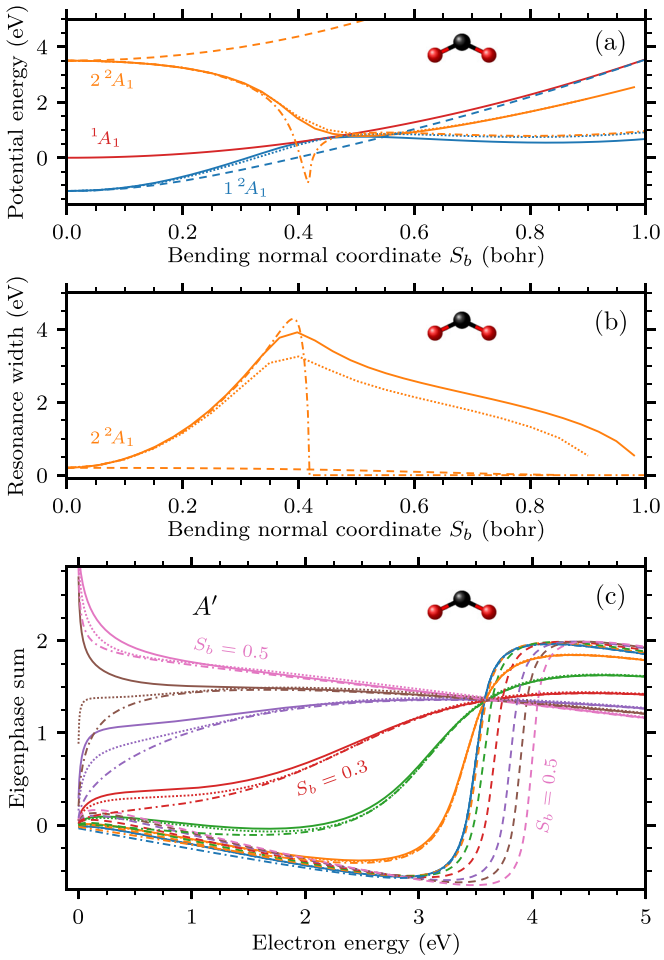

FIG. 8. Effect of model parameters describing the $\Sigma\Pi$ coupling on the $1\,^2A_1$ virtual state and $2\,^2A_1$ Renner-Teller component of the $^2\Pi_u$ resonance. Solid lines, full model; dotted lines, model with $\lambda = 0$; dashed lines, model with $v_{\Pi s} = 0$; dot-dashed lines, model without the Σ state (all relevant parameters are set to zero). Panels (a) and (b) show real part and width of the adiabatic potential energy surfaces upon bending ($S_g = 0$, $S_u = 0$). Panel (c) shows the A' model eigenphase sums for geometries $S_g = 0, S_u = 0, S_b = 0.0, 0.1, 0.2, 0.3, 0.4, 0.45$, and 0.5 bohrs.

C. Contribution of individual partial waves

Our R-matrix calculations include electron partial waves up to $l = 4$ while the model for the dynamics takes into account only $l = 0, 1$. There are no principal obstacles to include all the partial waves into the model, but it would immensely increase its complexity. By fitting the model to the full eigenphase sums we also included the information on higher partial waves into the model but the splitting of this information into partial waves is not captured correctly. We expect that this deficiency will have a small influence on the integral cross sections but it may harm the differential cross sections. To assess the possible effect of this approximation, we here discuss individual contributions of partial waves to *ab initio* K matrices. In what follows we refer to $\arctan[K_{\mu\mu}(\epsilon)]$ where $K_{\mu\mu}$ is the diagonal K-matrix element for a partial wave μ as to partial-wave phase.

In the A'' contribution, the model K matrix has just one element $K_{p_\perp p_\perp}(\epsilon)$ since the model includes only the $\Pi_\perp$ state

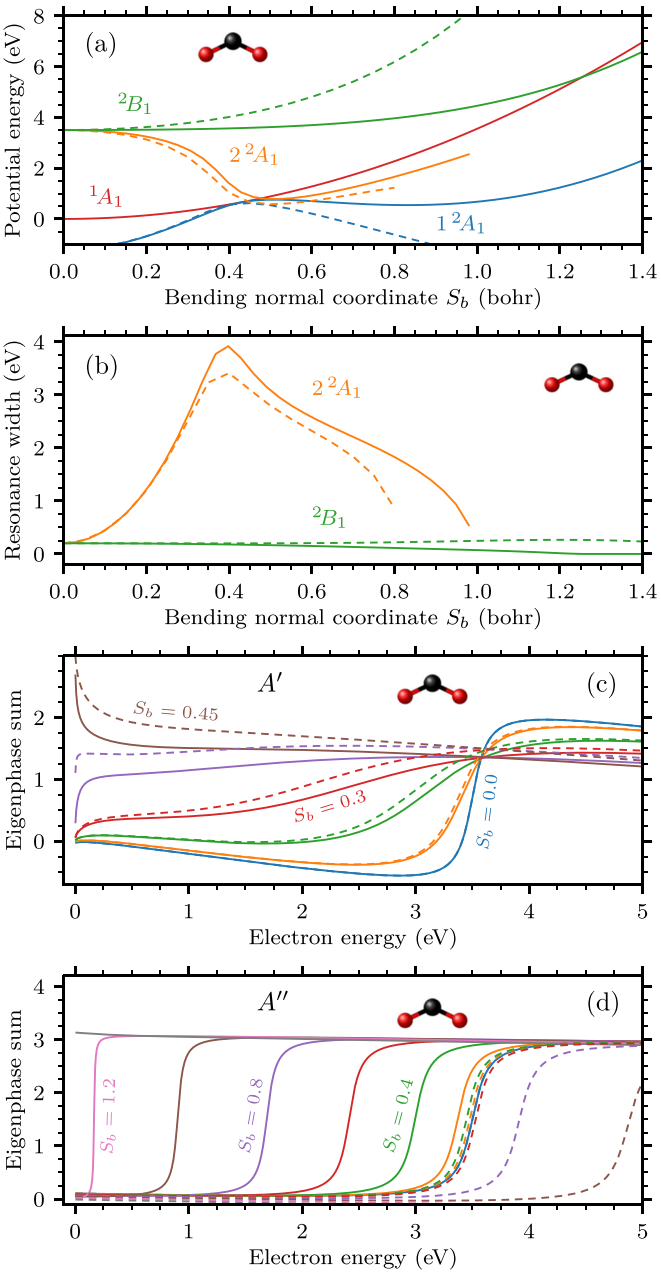

FIG. 9. Effect of the model parameter ξ describing the Renner-Teller coupling of the $^2\Pi_u$ shape resonance upon bending. Solid lines, full model; dashed lines, model with $\xi = 0$. Panels (a) and (b) show the real part and the width of the adiabatic potential energy surfaces upon bending ($S_g = 0$, $S_u = 0$). Panel (c) shows the A' model eigenphase sums for geometries $S_g = 0$, $S_u = 0$, $S_b = 0.0$, 0.1, 0.2, 0.3, 0.4, and 0.45 bohrs. Panel (d) shows the A'' model eigenphase sums for geometries $S_g = 0$, $S_u = 0$, $S_b = 0.0$, 0.2, 0.4, 0.6, 0.8, 1.0, 1.2, and 1.4 bohrs.

coupled to the $p_\perp$ electron partial wave. On the other hand, the *ab initio* K matrix contains ten contributions. The $p_\perp$ partial-wave phase dominantly contributes to the A'' *ab initio* eigenphase sums, but there is also a considerable contribution of one f-wave component and for nonzero bending a d wave is involved too (see Fig. 10), which is consistent with Morgan [21].

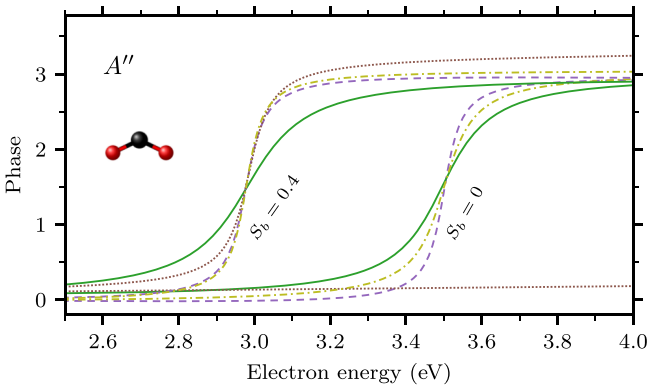

FIG. 10. Visualization of *ab initio* K-matrix elements for geometries $S_g = 0$, $S_u = 0$, $S_b = 0$ and 0.4 bohrs; solid lines, eigenphase sums; dashed lines, contribution of the $p_\perp$ partial wave; dotted lines, contribution of a d wave; dot-dashed lines, contribution of a f wave (see the text).

In the A' problem, the discrete-state (resonant) K matrix within our nonlocal model is a 3×3 matrix labeled by the partial waves s, p_z, $p_{||}$. It can be calculated using the Cayley transform [58] from the following T matrix:

$$T_{A'}(\epsilon) = \left(V_\epsilon^{A'}\right)^T (\epsilon - H_{A'})^{-1} V_\epsilon^{A'}, \tag{47}$$

where $H_{A'}$ and $V_\epsilon^{A'}$ are given by Eqs. (26) and (27), respectively. Upon bending, the s wave dominates and the model partial-wave phase is in a very good agreement with the *ab initio* phase; see Fig. 11(a). The discrepancy between the $p_{||}$-wave contributions is again caused by the fact that the

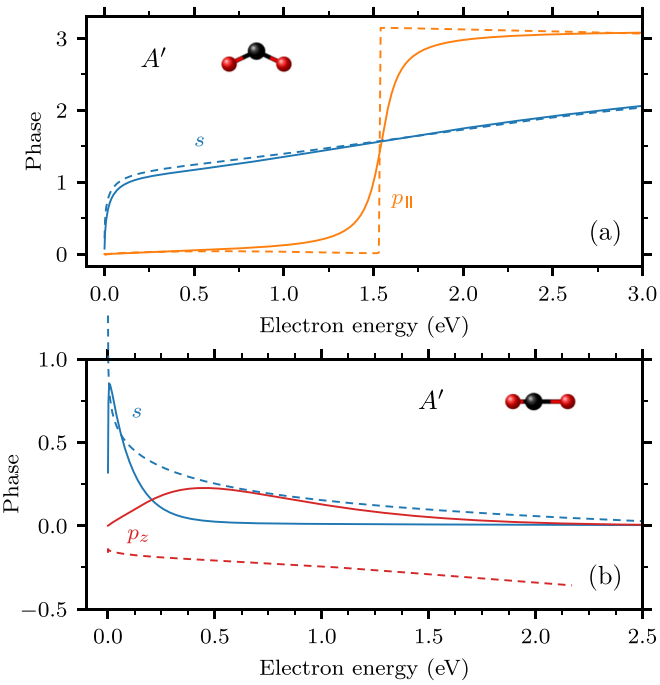

FIG. 11. Visualization of K-matrix elements; solid lines, our model; dashed lines, R-matrix data. (a) s and $p_{||}$-wave contributions for geometry $S_g = 0$, $S_u = 0$, $S_b = 0.4$ bohrs. (b) s- and p_z-wave contributions for geometry $S_g = 0$, $S_b = 0$, $S_u = 0.3$ bohrs.

model effectively describes also the higher partial waves. Figure 11(b) shows that the *s*-wave again dominates the *ab initio* data in the asymmetric stretching while p_z rather contributes to the background. The model *s* wave is not able to describe the *ab initio* data because of the limitations in our parametrization of the model; see Sec. IV B and IV C. By fitting the model to the eigenphase sums, it is difficult to get the behavior of the p_z wave consistent with the *R*-matrix data because of the background-like contribution and the model p_z wave tries to compensate the *s*-wave behavior. Therefore, we can not expect a very good agreement of our cross sections with experimental data for asymmetric stretching.

VI. VIBRONIC DYNAMICS

The final purpose of the theoretical treatment is to obtain the cross sections that can be compared to experiments or used in simulations of the inelastic electron scattering. The differential cross section for vibrational excitation can be computed by averaging the T matrix over molecular orientations [9]

$$\frac{d\sigma_{\nu_f\leftarrow\nu_i}}{d\Omega}(\epsilon,\theta)=\frac{8\pi^4}{\epsilon^2}\overline{|T_{\nu_f\mathbf{k}_f\leftarrow\nu_i\mathbf{k}_i}|^2}, \tag{48}$$

where the horizontal bar denotes the averaging and θ is a scattering angle. The T matrix $T_{\nu_f\mu_f\leftarrow\nu_i\mu_i}$ given by Eq. (7) and the T matrix $T_{\nu_f\mathbf{k}_f\leftarrow\nu_i\mathbf{k}_i}$ are related through partial-wave expansions

$$T_{\nu_f\mathbf{k}_f\leftarrow\nu_i\mathbf{k}_i}=\sum_{\mu_i,\mu_f}Y^*_{\mu_f}(\hat{\mathbf{k}}_f)T_{\nu_f\mu_f\leftarrow\nu_i\mu_i}Y_{\mu_i}(\hat{\mathbf{k}}_i), \tag{49}$$

where $\hat{\mathbf{k}}_i$ and $\hat{\mathbf{k}}_f$ denote the directions of the incoming and outgoing electrons in the molecular frame, respectively. To calculate the cross sections we consider only the discrete-state (resonant) T matrix, that is, we neglect the background contribution to all inelastic processes.

Since most experiments are conducted at room temperature where only the ground vibrational state of CO_2 is significantly populated, we consider only the ground state as the initial state ν_i in our calculations. Then the initial state of the CO_2 molecule (including the electronic degrees of freedom) is totally symmetric which implies that the symmetry of the initial asymptotic state of the e+CO_2 system is solely given by the symmetry of the incoming electron partial wave $\mu_i=(l_i,m_i)$. Consequently, the scattering wave function $|\Psi\rangle$, which satisfies the inhomogeneous Schrödinger equation

$$(E\mathbb{1}-H)|\Psi\rangle=V^{\mu_i}_{\epsilon_i}|\nu_i\rangle, \tag{50}$$

also has the symmetry of the incoming wave. The T matrix $T_{\nu_f\mu_f\leftarrow\nu_i\mu_i}$ given by Eq. (7), which can be written as the following integral:

$$T_{\nu_f\mu_f\leftarrow\nu_i\mu_i}=\langle\nu_f|V^{\mu_f\dagger}_{\epsilon_f}|\Psi\rangle, \tag{51}$$

is thus nonzero only when the product of representations of the final vibrational state ν_f and the final electron partial wave $\mu_f=(l_f,m_f)$ contains the irreducible representation of the initial partial wave, which restricts possible symmetries of the final vibrational states. Alternatively, we can determine the possible final states from conservation laws of angular momentum and parity. In our model, we take into account only rotations around the molecular axis associated with bending of the molecule. We denote the corresponding angular momentum quantum number by ℓ_b. Its values are then restricted by $m_i=m_f+\ell_b$, and we find that vibrational states of the Σ_g^+, Σ_u^+, Π_g, Π_u, and Δ_g symmetries can be excited in our model. The resulting formulas for the differential cross sections are derived in Appendix D, where the averaging of the T matrix over molecular orientations is explicitly performed for each symmetry of the final vibrational states.

The integral cross section for vibrational excitation is obtained by integrating over the solid angle Ω:

$$\sigma_{\nu_f\leftarrow\nu_i}(\epsilon)=\frac{2\pi^3}{\epsilon}\sum_{\mu_i,\mu_f}|T_{\nu_f\mu_f\leftarrow\nu_i\mu_i}|^2. \tag{52}$$

In our model, the vibrational states $|\nu_f\rangle$ are determined within the harmonic approximation Eq. (A8). However, anharmonic terms in the neutral potential of CO_2 cause a strong mixing between symmetric stretching and bending modes, the so-called Fermi resonance effect [45]. This effect is thus not included in our dynamics but can be incorporated to a good approximation by replacing the T matrix in the formulas for the cross sections by a proper linear combination of T matrices obtained using harmonic states [8]; see our Letter [18]. We will discuss this problem more in our follow-up paper.

A. Expansion of the dynamics in the oscillator basis

To obtain the T matrix given by Eq. (51) we solve the Schrödinger Eq. (50) for each μ_i independently with total energy E given by the conservation law Eq. (8). The vibronic wave function $|\Psi\rangle$ of the anion has three vibrational components $|\psi_d\rangle$, one for each discrete electronic state Σ and $\Pi_\pm$,

$$|\Psi\rangle=\begin{pmatrix}|\psi_{\Pi_+}\rangle\\|\psi_\Sigma\rangle\\|\psi_{\Pi_-}\rangle\end{pmatrix}. \tag{53}$$

Note that the dynamics reflects the full molecular symmetry group $D_{\infty h}$. The vibrational wave functions $|\psi_d\rangle$ compensate the symmetry of the discrete states so that $|\Psi\rangle$ has the total symmetry given by the incoming partial wave.

To solve the Schrödinger Eq. (50) we expand the components $|\psi_d\rangle$ into the four-dimensional oscillator basis that consists of eigenfunctions $|\nu_g,\nu_b,\ell_b,\nu_u\rangle$ of the neutral molecule Hamiltonian H_0 (the explicit form is given in Appendix A)

$$|\psi_d\rangle=\sum_{\nu_g,\nu_b,\ell_b,\nu_u}\psi_d(\nu_g,\nu_b,\ell_b,\nu_u)|\nu_g,\nu_b,\ell_b,\nu_u\rangle, \tag{54}$$

where $\psi_d(\nu_g,\nu_b,\ell_b,\nu_u)$ are the expansion coefficients. The basis expansion is truncated in the individual dimensions. We have $\nu_g=0,\ldots,N_g-1$, $\nu_u=0,\ldots,N_u-1$, and $\nu_b=0,\ldots,N_b-1$ for symmetric stretching, asymmetric stretching, and bending, respectively. The incoming electron brings utmost one quantum of the angular momentum but intermediate and final vibrational states can have up to $\ell_b=\pm2$. For that reason, it is sufficient to consider $\ell_b=0,\pm1,\pm2$.

By expressing the effective Hamiltonian H and the right-hand side $V^{\mu_i}_{\epsilon_i}|\nu_i\rangle$ in Eq. (50) in the same basis, we get a

system of linear equations $Ax = b$ for x representing the unknown coefficients $\psi_d(\nu_g, \nu_b, \ell_b, \nu_u)$. Although the number $N \propto N_g N_u N_b$ of the unknowns is large (typically $\sim 10^6$; see below), the resulting matrix A is sparse due to the restriction of the model functions to low-order polynomials in the normal coordinates. Thus, the linear system is, at least in principle, solvable by iterative matrix methods. Algorithms of these methods depend only on matrix-vector multiplications, that is, the explicit knowledge of the coefficient matrix A is not necessary. Hence, we implemented only the action of the Hamiltonian Eq. (5) on the nuclear wave function $|\Psi\rangle$. The action of the first term H_0 is trivial since the basis functions are the eigenstates of H_0. The action of the second term U given by Eq. (17) can be expressed in a straightforward way if we can act with operators Q_g, Q_u, $Q_\pm$, ρ^2 on the components $|\psi_d\rangle$. The first two operators are represented by tridiagonal matrices acting only on one index ν_g or ν_u, respectively. Similarly, operators $Q_\pm$ and ρ^2 act in a simple manner only on indexes ν_b and ℓ_b. For details see Appendix A.

On the other hand, the third term $F(E - H_0)$ is an operator function of H_0 and its action via Eq. (6) deserves to be explained in more detail. The continuum coupling elements $V^\mu_{d\epsilon}$ were constructed to be separable in space and energy variables

$$V^\mu_{d\epsilon}(\vec{q}\,) = \mathcal{A}^\mu_d(\vec{q}\,)\zeta^\mu_d(\epsilon), \tag{55}$$

where $\zeta^\mu_d(\epsilon) = (\beta\epsilon)^{(2l+1)/4}\exp(-\beta\epsilon)$ depends only on energy [see Eq. (44)], $\mathcal{A}^\mu_d(\vec{q}\,)$ includes the polynomial a from Eq. (44) and in some cases also $Q_\pm$ or Q_u; see Eq. (18). By substituting the separated form Eq. (55) into Eq. (19), we get

$$F_{dd'}(E - H_0) = \sum_\mu \mathcal{A}^\mu_d(\vec{q}\,) f^\mu_{dd'}(E - H_0)\mathcal{A}^\mu_{d'}(\vec{q}\,), \tag{56a}$$

where

$$f^\mu_{dd'}(E - H_0) = \text{v.p.}\int_0^\infty d\epsilon \frac{\zeta^\mu_d(\epsilon)\zeta^\mu_{d'}(\epsilon)}{E - H_0 - \epsilon} - i\pi\,\zeta^\mu_d(E - H_0)\zeta^\mu_{d'}(E - H_0). \tag{56b}$$

The order of the operators in the sum above is important since the normal coordinates do not commute with H_0. Some $V^\mu_{d\epsilon}$ terms are given by several separable terms; for example, see Eq. (40). The generalization of the formulas above for such cases is straightforward.

The $F_{dd'}(E - H_0)$ operators act on a vibrational wave function $|\psi\rangle$ in the oscillator basis in the following way:

$$\langle\nu|F_{dd'}(E - H_0)|\psi\rangle = \sum_{\mu,\nu',\nu''} \langle\nu|\mathcal{A}^\mu_d|\nu''\rangle f^\mu_{dd'}(E - E_{\nu''}) \times \langle\nu''|\mathcal{A}^\mu_{d'}|\nu'\rangle\psi(\nu'), \tag{57}$$

where ν, ν', and ν'' are multi-indices $(\nu_g, \nu_b, \ell_b, \nu_u)$. The action of $F_{dd'}$ corresponds to a multiplication of a vector by three matrices. The energy matrix $f^\mu_{dd'}(E - E_{\nu''})$ is diagonal because of the harmonic approximation for the neutral molecule and the multiplication by matrices $\mathcal{A}^\mu_d$ can be decomposed to action of the coordinate operators Q_g, Q_u, $Q_\pm$ which significantly simplifies the evaluation.

In total, the action of the sparse matrix A that represents $E\mathbb{1} - H$ on a vector v requires cN operations rather then N^2 operations required for a general matrix of the same size, where c is a small number depending on the complexity of our model but independent of the basis size N.

B. Numerical solution

The matrix A representing the $E\mathbb{1} - H$ operator is complex symmetric but not Hermitian, and thus, the conjugate gradient method [60] can not be used. Instead, we used its generalization, the conjugate orthogonal conjugate gradient method (COCG), proposed by van der Vorst and Melissen [61].

The COCG method converges rather quickly for small electron energies but not even 10^5 iterations were sufficient for achieving the convergence above 2.5 eV. We found out that the COCR [62], BiCG [63], and BiCGStab [64] methods exhibit a similar behavior. Finding a suitable preconditioner that improves the rate of convergence is thus necessary. Physically motivated preconditioners based on freezing some of the vibrational modes did not turn out to be viable. In the end, we came up with a rather standard preconditioner using the LU decomposition which significantly improves the rate of convergence. Let us write the matrix A in the following form:

$$A = \sum_{d,d',\nu,\nu'} |\nu\rangle|d\rangle A_{d\nu,d'\nu'}\langle d'|\langle\nu'|, \tag{58}$$

where d, d' run over the discrete states, ν, ν' run over vibrational quantum numbers ν_g, ν_b, ℓ_b, and ν_u. Then we consider only diagonal blocks in the stretching modes for the matrix P of the preconditioner

$$P = \sum_{d,d',\nu,\nu'} |\nu\rangle|d\rangle\delta_{\nu_g\nu'_g}\delta_{\nu_u\nu'_u}A_{d\nu,d'\nu'}\langle d'|\langle\nu'|. \tag{59}$$

In the other words, P is block diagonal with the blocks including the discrete-state space in combination with only the bending mode. Applying the preconditioner to a vector v corresponds to solving a linear system $Py = v$, which can be done for each block separately using the LU decomposition.

The construction of the matrix P is somewhat challenging since we have to explicitly evaluate the matrix A. The action of A on the ith basis vector provides the ith column of A. To act by A on all basis vectors is very time consuming; however, it can be greatly optimized when we realize the Hamiltonian spreads the nonzero basis component to only nearby components because of the polynomial structure of H. Therefore, we can act by A on a small section of basis vectors and speed up the calculation.

In total, we solved the vibrational dynamics for each incoming electron partial wave for 1500 electron energies from 0.001 eV up to 5 eV. The basis size has to be increased for larger energies since the anion can probe more of the potential energy surfaces, which is especially true in the bending dimension; see Fig. 4. The final basis sizes used are listed in Table I. The iterations were stopped when the ratio of norms of the residua and right-hand side b was smaller than a tolerance $\tau = 10^{-3}$. The convergence of the cross sections with respect to both the basis size and tolerance τ was tested. The calculations can be easily parallelized over electron energies. The calculation for 1 eV took approximately 600 seconds on one CPU core, and the convergence without the preconditioning was achieved after about 1000 iterations. The preconditioning was essential above 2.5 eV. For 3 eV we needed 200 iterations

TABLE I. Basis sizes used in the dynamics for given ranges of electron energies; N_g, N_u, and N_b give the number of basis functions in symmetric stretching, asymmetric stretching, and bending, respectively; N_e is the number of calculated electron energies.

Energies (eV)	N_g	N_b	N_u	N_e
0.001–1.0	30	60	20	500
1.0–2.0	30	80	20	400
2.0–3.0	30	100	20	300
3.0–4.0	35	120	25	200
4.0–5.0	40	140	30	100

and an hour of computational time, and finally, 1800 iterations were necessary for 5 eV with around 9 hours of the elapsed time, from which the construction of the preconditioner took a half of the time.

VII. CONCLUSION

In this paper, we have presented our nonlocal model describing the nuclear dynamics of the vibrational excitation of the CO_2 molecule by low-energy electrons. The model includes the mutually interacting $^2\Sigma_g^+$ virtual state and the Renner-Teller coupled $^2\Pi_u$ shape resonance of the CO_2^- in combination with all four vibrational modes. The general form of the direct discrete-state coupling matrix and discrete-state-continuum coupling matrix resulting from the $D_{\infty h}$ symmetry group has been derived. The construction of the model from our R-matrix eigenphase sums and potential energies has been described in detail. Although the model contains a large number of parameters, the symmetry considerations significantly simplify the fitting process. We have shown that the explicit inclusion of the coupling of the lower Renner-Teller component to the electronic s-wave continuum explains the peculiar behavior of this state. Moreover, we have discussed the origin of the nonlinear potential minimum of the ground state of CO_2^-. We have proposed the numerical treatment of the dynamics based on preconditioned Krylov subspace methods suitable for a large class of nonlocal discrete-state-in-continuum models and we have demonstrated its feasibility for the four-dimensional dynamics within the present model.

In order to be able to solve the multidimensional dynamics, we have made several approximations. Most notably, we have used only the harmonic approximation for the neutral molecule (description of the molecular anion includes anharmonic terms) and constant threshold exponents, which prevent the description of a geometry-dependent dipole moment. Despite the fact that the harmonic approximation leads to a quantitative disagreement between the model and *ab initio* potentials in the symmetric stretching vibrational mode, the model captures primary features of the system and provides an interpretation of unexplained observations in the electron scattering off CO_2; see the outlined discussion in our Letter [18]. In our follow-up to this paper, we will extend the discussion of our results and their comparison with experimental data including also effects of model parameters described here.

The application of the present theoretical treatment to other polyatomic systems is rather straightforward. The model structure is the consequence of the symmetry of the involved discrete electronic states and vibrational modes, and the dynamics allows excitation of nontotally symmetric vibrations. Such vibrations have been known to be excited by resonant processes for a long time, at least since measurements of Wong and Schulz [65], who also formulated selection rules based on symmetry considerations. These rules were later thoroughly discussed by Gallup [66,67] but actual dynamical calculations are scarce. Čurík *et al.* [68,69] studied vibrational excitation of diacetylene and cyclopropane molecules using the *ab initio* discrete momentum representation method and they even reported breaking of the selection rules in the case of the cyclopropane. We thus hope that the presented approach can bring additional insight into the multimode vibronic dynamics and explain spectra of other polyatomic systems. However, the model construction from *ab initio* data and solution of the dynamics remain to be challenging.

Several improvements of the model are possible. First, the approximations we have made can be lifted at the cost of a more complicated evaluation of the nonlocal potential $F(E - H_0)$. In the case of a geometry-dependent dipole, the Bateman approximation [70] has been successfully used to simplify the nonlocal dynamics [55,71]. Second, our model does not allow for the description of the dissociative electron attachment process. The form of discrete-state potentials based on polynomials in vibrational coordinates, which is essential for producing the sparse linear system for the dynamics, prevents straightforward implementation of a dissociative attachment channel. On the other hand, the incorporation of at least one dissociative channel is desirable for future development of the present approach.

ACKNOWLEDGMENTS

We gratefully acknowledge the financial support provided by the Czech Science Foundation under project No. 19-20524S and by the Charles University Grant Agency, Project No. 552120.

APPENDIX A: VIBRATIONAL COORDINATES AND HARMONIC OSCILLATOR BASIS

Here we define normal coordinates S_g, S_u, S_x, and S_y of symmetric stretching, antisymmetric stretching, and two-dimensional bending, respectively. We used Witteman's definition [42] with one minor modification. We changed the sign of S_g so that positive values correspond to the lengthening of the C–O bond and not to its shortening. The molecular axis at the equilibrium geometry coincides with the z axis with the carbon atom being at the origin. The Cartesian coordinates of the atoms expressed in terms of the normal coordinates are

$$\vec{R}_C \equiv (x_C, y_C, z_C) = -\frac{2m_O}{M}(S_x, S_y, S_u), \tag{A1}$$

$$\vec{R}_{O1} = \left[\frac{S_g}{2} + R_{CO}\right](0, 0, -1) + \frac{m_C}{M}(S_x, S_y, S_u), \tag{A2}$$

$$\vec{R}_{O2} = \left[\frac{S_g}{2} + R_{CO}\right](0, 0, 1) + \frac{m_C}{M}(S_x, S_y, S_u), \tag{A3}$$

where $m_C = 21\,874.66\,m_e$ is the mass of the carbon atom in the electron mass, $m_O = 29\,156.95\,m_e$ is the oxygen mass, $M = m_C + 2m_O$ is the total mass of CO_2, and $R_{CO} = 2.1961$ bohr is the experimental equilibrium distance of the carbon-oxygen bond. The dimensionless normal coordinates are given by [42]

$$Q_g = \sqrt{\frac{\mu_1\omega_g}{\hbar}}S_g, \quad Q_u = \sqrt{\frac{\mu_2\omega_u}{\hbar}}S_u, \tag{A4}$$

$$Q_x = \sqrt{\frac{\mu_2\omega_b}{\hbar}}S_x, \quad Q_y = \sqrt{\frac{\mu_2\omega_b}{\hbar}}S_y, \tag{A5}$$

where ω_g, ω_u, and ω_b are the angular frequencies of the symmetric stretching, antisymmetric stretching and bending, respectively, $\mu_1 = m_O/2$, and $\mu_2 = 2m_Om_C/M$.

The neutral molecule Hamiltonian in the harmonic approximation is then written as $H_0 = T_N + V_0$ with

$$T_N = -\frac{1}{2}\omega_g\frac{\partial^2}{\partial Q_g^2} - \frac{1}{2}\omega_u\frac{\partial^2}{\partial Q_u^2} - \frac{1}{2}\omega_b\left(\frac{\partial^2}{\partial\rho^2} + \frac{1}{\rho}\frac{\partial}{\partial\rho} + \frac{1}{\rho^2}\frac{\partial^2}{\partial\varphi^2}\right), \tag{A6a}$$

$$V_0 = \frac{1}{2}\omega_g Q_g^2 + \frac{1}{2}\omega_b\rho^2 + \frac{1}{2}\omega_u Q_u^2, \tag{A6b}$$

where polar coordinates ρ and φ are defined in Eq. (9).

To solve the vibronic dynamics we expand each discrete-state component $\psi_d(\vec{q}\,)$ in the basis of vibrational eigenfunctions of the neutral molecule [see Eq. (54)] and implement the action of the Hamiltonian Eq. (5) on the expansion coefficients. The basis is thus defined by relation $H_0|\nu\rangle = E_\nu|\nu\rangle$ with

$$E_\nu = \omega_g(\nu_g + 1/2) + \omega_b(\nu_b + 1) + \omega_u(\nu_u + 1/2), \tag{A7}$$

where we use a shorthand notation $\nu \equiv (\nu_g, \nu_b, \ell_b, \nu_u)$. The basis wave functions $\langle\vec{q}\,|\nu\rangle$ are given by the product of wave functions of one-dimensional harmonic oscillators in the stretching modes and two-dimensional harmonic oscillator in the bending motion which read in x representation [72]

$$\langle\vec{q}\,|\nu_g, \nu_b, \ell_b, \nu_u\rangle = \phi_{\nu_g}(Q_g)\Phi_{\nu_b\ell_b}(\rho,\varphi)\phi_{\nu_u}(Q_u) \tag{A8a}$$

with

$$\phi_n(q) = \left(\sqrt{2^n n!\sqrt{\pi}}\right)^{-1} H_n(q)e^{-q^2/2}, \tag{A8b}$$

$$\Phi_{n\ell}(\rho,\varphi) = \frac{1}{\sqrt{2\pi}}\sqrt{\frac{2n_r!}{(n_r+|\ell|)!}}\rho^{|\ell|}L_{n_r}^{|\ell|}(\rho^2)e^{i\ell\varphi}e^{-\rho^2/2}, \tag{A8c}$$

where $n = \nu_g$ or ν_u, $q = Q_g$ or Q_u, $H_n(q)$ are the Hermite polynomials, $L_{n_r}^{|\ell|}(\rho^2)$ are the generalized Laguerre polynomials, $n_r = \frac{1}{2}(n - |\ell|)$, and $\ell = -n, -n+2, \ldots, n$.

For evaluation of the action of operators U and F we need to act with operators of the normal coordinates Q_g, Q_u, and $Q_\pm$ on the wave functions. The coordinates Q_g and Q_u are represented in the one-dimensional oscillator basis by the well-known matrix

$$\langle n'|Q_{g,u}|n\rangle = \left(\sqrt{n}\,\delta_{n'n-1} + \sqrt{n+1}\,\delta_{n'n+1}\right)/\sqrt{2}, \tag{A9}$$

where $n = \nu_g$ and ν_u, respectively. For the coordinates $Q_\pm$ and $\rho^2 = Q_+Q_-$, we have in the two-dimensional basis [37]

$$\langle n', \ell'|Q_\pm|n, \ell\rangle = \pm\frac{1}{\sqrt{2}}\delta_{\ell'\ell\pm1}s_\pm(\ell) \times\left[\sqrt{n\pm\ell+2}\,\delta_{n'n+1} - \sqrt{n\mp\ell}\,\delta_{n'n-1}\right], \tag{A10}$$

where

$$s_+(\ell) = \begin{cases}+1 & \text{for } \ell \geqslant 0\\ -1 & \text{for } \ell < 0\end{cases}, \quad s_-(\ell) = \begin{cases}+1 & \text{for } \ell > 0\\ -1 & \text{for } \ell \leqslant 0\end{cases}, \tag{A11}$$

$$\langle n', \ell'|\rho^2|n, \ell\rangle = \delta_{\ell'\ell}(n+1)\,\delta_{n'n} - \tfrac{1}{2}\delta_{\ell'\ell}\left[\sqrt{n^2-\ell^2}\,\delta_{n'n-2} + \sqrt{(n+2)^2-\ell^2}\,\delta_{n'n+2}\right]. \tag{A12}$$

The formulas above can be derived using creation and annihilation operators for right and left circular quanta [72]. Higher powers of the coordinates are obtained in terms of matrix multiplication.

APPENDIX B: EIGENPHASE SUM FOR TWO-STATE PROBLEM

Let us consider two discrete states that belong to the same irreducible representation of a molecular point group and are coupled to an arbitrary number of electron partial waves. In general, the fixed-nuclei Hamiltonian within the discrete-states-in-continuum model then reads

$$H = U + F(\epsilon) = \begin{pmatrix}U_{11}+F_{11}(\epsilon) & U_{12}+F_{12}(\epsilon)\\ U_{12}+F_{12}(\epsilon) & U_{22}+F_{22}(\epsilon)\end{pmatrix}, \tag{B1}$$

where $F_{dd'}(\epsilon)$ are calculated analogically to Eq. (6). Note that we shifted the Hamiltonian with respect to, for example, Eq. (26) by subtracting V_0 so that it corresponds to the electron energy $\epsilon = E - V_0$ relative to threshold at given geometry. The fixed-nuclei T-matrix element for incoming μ_i and outgoing μ_f partial waves is given by

$$T_{\mu_f\leftarrow\mu_i} = \sum_{d,d'=1}^{2} V_{d\epsilon_f}^{\mu_f *}(\epsilon\mathbb{1}_2 - H)^{-1}_{dd'}V_{d'\epsilon_i}^{\mu_i}. \tag{B2}$$

We observe that T matrix is a rank-two operator in the space of partial waves μ. By denoting the vector of $V_{d\epsilon}^{\mu}$ amplitudes in the partial wave index μ by $|v_d\rangle$, we can write the S matrix in the form

$$S = \mathcal{I} - 2\pi i\sum_{d,d'=1}^{2}|v_d\rangle(\epsilon\mathbb{1}_2 - H)^{-1}_{dd'}\langle v_{d'}|, \tag{B3}$$

which implies that the S matrix has only two nontrivial eigenvalues $s = e^{2i\delta} \neq 1$, that is, there are only two nontrivial eigenphases $\delta \neq 0$. Thus, we can write eigenvectors as a linear combination of vectors $|v_d\rangle$, $|s\rangle = \sum_d c_d|v_d\rangle$. By projecting $\langle v_d|$ on the eigenproblem

$$S|s\rangle = s|s\rangle, \tag{B4}$$

TABLE II. Obtained values of the parameters of the matrix U. The parameters are polynomials $\sum_{i=0}^{4} c_i Q_g^i$ in the symmetric stretching normal coordinate Q_g. The notation $x(y)$ means $x \times 10^y$, and values are in the hartree unit of energy E_h.

	c_0 (E_h)	c_1 (E_h)	c_2 (E_h)	c_3 (E_h)	c_4 (E_h)
E_Π^0	0.13229(0)	−0.20130(−1)	0.40310(−3)	0	0
E_Π^{2b}	−0.37108(−3)	0.39684(−3)	0.23170(−4)	0	0
E_Π^{2u}	0.12675(−2)	−0.31060(−5)	0.22870(−6)	0	0
E_Π^{4b}	0.17624(−4)	0.12929(−4)	0.42013(−5)	0	0
E_Σ^0	0.40000(0)	0	0	0	0
E_Σ^{2b}	0.88740(−2)	−0.22622(−2)	0.75278(−3)	−0.18248(−3)	0.14277(−4)
E_Σ^{2u}	0.46670(−1)	−0.66847(−2)	0.19314(−3)	−0.17239(−3)	0.15079(−4)
E_Σ^{4b}	−0.31629(−4)	0.11550(−4)	−0.86640(−6)	0	0
E_Σ^{4u}	0.19697(−2)	−0.67839(−3)	0.62488(−4)	0	0
E_Σ^{4bu}	0.39880(−2)	−0.44038(−5)	−0.42582(−4)	0	0
λ	−0.77277(−2)	−0.80054(−5)	−0.59084(−3)	0	0
g	0.14523(−2)	0.28492(−3)	0.23170(−4)	0	0
κ	0.12134(−4)	0.13003(−4)	0.42013(−5)	0	0

we get the following equation for the coefficients c_d:

$$\sum_{d'=1}^{2} (\tilde{S}_{dd'} - s\Gamma_{dd'})c_{d'} = 0, \tag{B5}$$

where $\Gamma_{dd'} = -2\,\mathrm{Im}\,F_{dd'} = 2\pi \sum_\mu V_{d\epsilon}^\mu V_{d'\epsilon}^\mu = 2\pi \langle v_d | v_{d'} \rangle$ and (after some algebraic manipulations and realization that $H_{dp} + i\Gamma_{dp} = H_{dp}^*$)

$$\tilde{S}_{dd'} = \sum_{p,q=1}^{2} (\epsilon\delta_{dp} - H_{dp}^*)(\epsilon \mathbb{1}_2 - H)_{pq}^{-1} \Gamma_{qd'}. \tag{B6}$$

The condition for the existence of a nontrivial solution of Eq. (B5) is

$$\det(\tilde{S} - s\Gamma) = 0, \tag{B7}$$

which leads to a quadratic equation for the eigenvalues s_1 and s_2, and we can obtain the eigenphase sum $\delta_1 + \delta_2$ from the constant coefficient of the quadratic equation

$$s_1 s_2 = e^{2i(\delta_1+\delta_2)} = \frac{(\epsilon - H_{11}^*)(\epsilon - H_{22}^*) - (H_{12}^*)^2}{(\epsilon - H_{11})(\epsilon - H_{22}) - H_{12}^2}, \tag{B8}$$

which is equivalent to Eq. (30).

APPENDIX C: MODEL PARAMETERS

Here we list numerical values of the model parameters obtained from our fitting of the model to the R-matrix data. The parameter values of the matrix U, which is given by Eqs. (17), (37)–(39), are listed in Table II.

The continuum-coupling matrix V_ϵ is given by Eqs. (18), (40)–(42) and the parameters are of the form $v(\epsilon)$ Eq. (44). Actually, the parameter $v_{\Pi p}^{2b}$ that appears in Eq. (40) is given by the sum of two terms $v(\epsilon)$, $v_{\Pi p}^{2b} = v_{\Pi p}^{2b1} + v_{\Pi p}^{2b2}$, and similarly, $w_{\Pi p}$ in Eq. (18) is given by $w_{\Pi p} = w_{\Pi p}^1 + w_{\Pi p}^2$. The reason is the following. The model was constructed in the A'' and A' symmetries which depend on $v_{\Pi p}^{2b} - w_{\Pi p}$ and $v_{\Pi p}^{2b} + w_{\Pi p}$, respectively. These terms were independently parametrized by functions of the form $v(\epsilon)$. Thus, when we express $v_{\Pi p}^{2b}$ and $w_{\Pi p}$, we get two $v(\epsilon)$ terms. The obtained parameter values of the V_ϵ matrix are listed in Table III.

Finally, the parameter values of the background eigenphase sums, which are given by Eqs. (45) and (46), are listed in Table IV.

APPENDIX D: DIFFERENTIAL CROSS SECTIONS

The differential cross section for vibrational excitation of a molecule from the initial vibrational state ν_i to final state ν_f by an electron with the initial $\mathbf{k}_i$ and final $\mathbf{k}_f$ momenta is given by averaging the T matrix over molecular orientations [9]

$$\frac{d\sigma_{\nu_f \leftarrow \nu_i}}{d\Omega}(\epsilon, \theta) = \frac{8\pi^4}{\epsilon^2} \overline{|T_{\nu_f \mathbf{k}_f \leftarrow \nu_i \mathbf{k}_i}|^2}, \tag{D1}$$

where the discrete-state (resonant) contribution to the T matrix within the nonlocal model reads [15]

$$T_{\nu_f \mathbf{k}_f \leftarrow \nu_i \mathbf{k}_i} = \langle \nu_f | V_{\mathbf{k}_f}^\dagger (E\mathbb{1} - H)^{-1} V_{\mathbf{k}_i} | \nu_i \rangle. \tag{D2}$$

The discrete-state-continuum coupling $V_\mathbf{k}$ is a vector in the discrete-state index d. By expanding its elements into partial waves $\mu = (l, m)$

$$V_{d\mathbf{k}} = \sum_\mu V_{d\epsilon}^\mu Y_\mu(\hat{\mathbf{k}}), \tag{D3}$$

we get

$$T_{\nu_f \mathbf{k}_f \leftarrow \nu_i \mathbf{k}_i} = \sum_{\mu_i, \mu_f} Y_{\mu_f}^*(\hat{\mathbf{k}}_f) T_{\nu_f \mu_f \leftarrow \nu_i \mu_i} Y_{\mu_i}(\hat{\mathbf{k}}_i) \tag{D4}$$

with

$$T_{\nu_f \mu_f \leftarrow \nu_i \mu_i} = \langle \nu_f | V_{\epsilon_f}^{\mu_f \dagger} (E\mathbb{1} - H)^{-1} V_{\epsilon_i}^{\mu_i} | \nu_i \rangle. \tag{D5}$$

TABLE III. Obtained values of the parameters of the continuum-coupling matrix V_ϵ. The parameters has the form of Eq. (44) with the parameter a being a polynomial $\sum_{i=0}^{2} c_i Q_g^i$ in the symmetric stretching normal coordinate Q_g. The notation $x(y)$ means $x \times 10^y$, and E_h is the hartree unit of energy.

	c_0 $(E_h^{1/2})$	c_1 $(E_h^{1/2})$	c_2 $(E_h^{1/2})$	l	β (E_h^{-1})
$v^0_{\Sigma s}$	0.15505(0)	0.40072(−1)	0.88177(−3)	0	0.14586(2)
$v^{2b}_{\Sigma s}$	0.86210(−2)	−0.25939(−2)	0.17858(−3)	0	0.28841(2)
$v^{2u}_{\Sigma s}$	0.50983(−1)	−0.85719(−2)	0.17197(−3)	0	0.20000(3)
$v^0_{\Pi s}$ [a]	0.62981(−1)	0.27292(−2)	−0.18793(−3)	0	0.88654(0)
$v^{2u}_{\Pi s}$	−0.24927(−3)	0.53192(−4)	0.12654(−4)	0	0.40101(2)
$v^0_{\Pi p}$	0.10265(0)	−0.11894(−1)	0.57839(−3)	1	0.29575(1)
$v^{2b1}_{\Pi p}$	−0.44586(−2)	−0.27871(−2)	−0.14301(−5)	1	0.21098(0)
$v^{2b2}_{\Pi p}$	0.91958(−4)	0.24018(−4)	0.11016(−5)	1	0.33418(2)
$v^{2u}_{\Pi p}$	0.16151(−2)	−0.32262(−4)	−0.86390(−6)	1	0.33815(1)
$w^1_{\Pi p}$	−0.44586(−2)	−0.27871(−2)	−0.14301(−5)	1	0.21098(0)
$w^2_{\Pi p}$	−0.91958(−4)	−0.24018(−4)	−0.11016(−5)	1	0.33418(2)
$v_{\Pi z}$	0.10947(−1)	0.14344(−2)	−0.24540(−3)	1	0.15189(2)
$v_{\Sigma p}$	0.29400(−1)	−0.11984(−2)	−0.24803(−2)	1	0.19498(2)
$v_{\Sigma z}$	0.22929(0)	−0.11758(−1)	−0.34163(−2)	1	0.41721(2)

[a]The $v^0_{\Pi s}$ parameter has also terms of the third and fourth order with coefficients $c_3 = -0.42421(-4)$ $E_h^{1/2}$ and $c_4 = -0.51748(-5)$ $E_h^{1/2}$.

Then we can perform the averaging over the molecular orientations using Euler angles α, β, γ:

$$\frac{d\sigma_{v_f \leftarrow v_i}}{d\Omega}(\epsilon, \theta) = \frac{f(\epsilon)}{8\pi^2} \int_0^{2\pi} d\alpha \int_0^{2\pi} d\gamma \int_0^{\pi} d\beta \sin\beta \left| \mathcal{R}(\alpha, \beta, \gamma) \sum_{l_i, m_i} \sum_{l_f, m_f} Y^*_{l_f m_f}(\hat{\mathbf{k}}_f) T_{v_f l_f m_f \leftarrow v_i l_i m_i} Y_{l_i m_i}(\hat{\mathbf{k}}_i) \right|^2, \tag{D6}$$

where $\mathcal{R}(\alpha, \beta, \gamma)$ is the corresponding rotational operator and $f(\epsilon) = \pi^2/(2\epsilon)$. The rotational operator $\mathcal{R}$ acts on the direction vectors $\hat{\mathbf{k}}_i$ and $\hat{\mathbf{k}}_f$ of the initial and final electron momenta via the rotational matrix R:

$$R(\alpha, \beta, \gamma) = \begin{pmatrix} \cos\alpha & \sin\alpha & 0 \\ -\sin\alpha & \cos\alpha & 0 \\ 0 & 0 & 1 \end{pmatrix} \begin{pmatrix} \cos\beta & 0 & \sin\beta \\ 0 & 1 & 0 \\ -\sin\beta & 0 & \cos\beta \end{pmatrix} \begin{pmatrix} \cos\gamma & \sin\gamma & 0 \\ -\sin\gamma & \cos\gamma & 0 \\ 0 & 0 & 1 \end{pmatrix}, \tag{D7}$$

TABLE IV. Obtained values of the parameters of the background eigenphase sums. The parameters are polynomials $\sum_{i=0}^{4} c_i Q_g^i$ in the symmetric stretching normal coordinate Q_g. The coefficients of the $a_{\rm bg}$, $c_{\rm bg}$, $c^{1b}_{\rm bg}$, and $c^{2u}_{\rm bg}$ parameters are in units of E_h^{-1}, where E_h is the hartree unit of energy, and the rest of the parameters are dimensionless. The notation $x(y)$ means $x \times 10^y$.

	c_0	c_1	c_2	c_3	c_4
$a_{\rm bg}$	−0.11585(1)	0.20994(−1)	0.36453(−3)	0	0
$b_{\rm bg}$	0.10443(0)	−0.10081(−2)	−0.11098(−3)	0	0
$b^{2b}_{\rm bg}$	−0.90841(−3)	0.12924(−6)	0.19154(−7)	0	0
$b^{2u}_{\rm bg}$	0.15270(−2)	−0.16398(−3)	0	0	0
$c_{\rm bg}$	−0.63794(1)	0.61145(0)	0.83917(−1)	0	
$c^{1b}_{\rm bg}$	−0.11542(−1)	−0.62076(−1)	−0.16750(−1)	0.46431(−3)	0.49201(−3)
$c^{2u}_{\rm bg}$	0.72745(−1)	0.50706(−2)	−0.78337(−3)	0	0
$d_{\rm bg}$	−0.35235(−1)	0.77574(−2)	0.91983(−3)	0	0
$d^{1b}_{\rm bg}$	0.16629(−1)	−0.51348(−2)	0.11835(−2)	0.27039(−3)	−0.567215(−6)
$d^{2u}_{\rm bg}$	−0.16497(−2)	0.61585(−3)	0.17584(−3)	0	0
$d^{3bu}_{\rm bg}$	0.90811(−3)	0.73771(−6)	0.49481(−6)	−0.12696(−7)	0

that is, we have

$$\frac{d\sigma_{\nu_f\leftarrow\nu_i}}{d\Omega}(\epsilon,\theta)=\frac{f(\epsilon)}{8\pi^2}\int_0^{2\pi}d\alpha\int_0^{2\pi}d\gamma\int_0^{\pi}d\beta\sin\beta\sum_{l_i,m_i}\sum_{l_f,m_f}Y^*_{l_fm_f}(R\hat{\mathbf{k}}_f)T_{\nu_f l_f m_f\leftarrow\nu_i l_i m_i}Y_{l_im_i}(R\hat{\mathbf{k}}_i)$$
$$\times\sum_{l'_i,m'_i}\sum_{l'_f,m'_f}Y_{l'_fm'_f}(R\hat{\mathbf{k}}_f)T^*_{\nu_f l'_f m'_f\leftarrow\nu_i l'_i m'_i}Y^*_{l'_im'_i}(R\hat{\mathbf{k}}_i). \tag{D8}$$

In our model of the e+CO_2 system, we consider electron partial waves $\mu=(l,m)=(0,0)$, (1,0), and $(1,\pm1)$ for the s, p_z, and $p_\pm$ partial waves in the expansion Eq. (D3). The corresponding spherical harmonic functions Y_μ are

$$Y_{00}=1/\sqrt{4\pi},\quad Y_{10}=\sqrt{3/(4\pi)}k_z,\quad Y_{1\pm1}=\mp\sqrt{3/(8\pi)}(k_x\pm ik_y), \tag{D9}$$

where k_x, k_y, k_z are the Cartesian components of the electron momentum direction vector. In addition, we consider only the initial vibrational state ν_i to be the ground vibrational state of CO_2, and thus, the symmetry of the final vibrational state ν_f restricts possible combinations of the incoming and outgoing partial waves; see Sec. VI. Without loss of generality, we set $\hat{\mathbf{k}}_i=(0,0,1)^T$ and $\hat{\mathbf{k}}_f=(\sin\theta,0,\cos\theta)^T$, where θ is a scattering angle. The integration over the Euler angles results in the following formulas for Σ_g^+, Σ_u^+, Π_g, Π_u, and Δ_g final vibrational states:

$$\frac{d\sigma}{d\Omega}(\epsilon,\theta)\bigg|_{\Sigma_g^+}=f(\epsilon)\bigg\{|T_{ss}|^2+\frac{3}{5}(1+2\cos^2\theta)|T_{zz}|^2+\frac{3}{10}(3+\cos^2\theta)(|T_{++}|^2+|T_{--}|^2)+2\cos\theta\,\mathrm{Re}\,[T_{ss}(T^*_{++}+T^*_{--}+T^*_{zz})]$$
$$-\frac{3}{5}(1-3\cos^2\theta)[2\,\mathrm{Re}\,(T_{++}T^*_{--})+\mathrm{Re}\,(T_{zz}[T^*_{++}+T^*_{--}])]\bigg\}, \tag{D10}$$

$$\frac{d\sigma}{d\Omega}(\epsilon,\theta)\bigg|_{\Sigma_u^+}=f(\epsilon)[|T_{sz}|^2+|T_{zs}|^2+2\cos\theta\,\mathrm{Re}\,(T_{sz}T^*_{zs})], \tag{D11}$$

$$\frac{d\sigma}{d\Omega}(\epsilon,\theta)\bigg|_{\Pi_g}=f(\epsilon)\frac{3}{5}[(2-\cos^2\theta)(|T_{z+}|^2+|T_{-z}|^2+|T_{z-}|^2+|T_{+z}|^2)+(1-3\cos^2\theta)\,\mathrm{Re}(T_{z+}T^*_{-z}+T_{z-}T^*_{+z})], \tag{D12}$$

$$\frac{d\sigma}{d\Omega}(\epsilon,\theta)\bigg|_{\Pi_u}=f(\epsilon)\big[|T_{s+}|^2+|T_{-s}|^2+|T_{s-}|^2+|T_{+s}|^2-2\cos\theta\,\mathrm{Re}\,(T_{s+}T^*_{-s}+T_{s-}T^*_{+s})\big], \tag{D13}$$

$$\frac{d\sigma}{d\Omega}(\epsilon,\theta)\bigg|_{\Delta_g}=f(\epsilon)\frac{3}{10}(3+\cos\theta)(|T_{-+}|^2+|T_{+-}|^2), \tag{D14}$$

where we suppressed the ν_i and ν_f indices and used a shorthand notation for partial waves (l,m): s corresponds to (0,0), z to (1,0), and $\pm$ to $(1,\pm1)$.

Alternatively, we can calculate the differential cross sections by extending the derivation of McCurdy *et al.* [9], which leads to the following formula:

$$\frac{d\sigma_{\nu_f\leftarrow\nu_i}}{d\Omega}(\epsilon,\theta)=\frac{8\pi^4}{\epsilon}\sum_{l_i,m_i}\sum_{l'_i,m'_i}\sum_{l_f,m_f}\sum_{l'_f,m'_f}\frac{\sqrt{(2l_i+1)(2l'_i+1)}}{4\pi}T_{\nu_f l_f m_f\leftarrow\nu_i l_i m_i}T^*_{\nu_f l'_f m'_f\leftarrow\nu_i l'_i m'_i}\sum_{M=-l_f}^{l_f}Y^*_{l_fM}(\hat{\mathbf{k}}_f)Y_{l'_fM}(\hat{\mathbf{k}}_f)$$
$$\times\sum_{j=|l_f-l'_i|}^{l_f+l'_i}\sum_{m=-j}^{j}(2j+1)\begin{pmatrix}l_f & l'_i & j\\ M & 0 & -M\end{pmatrix}\begin{pmatrix}l'_f & l_i & j\\ M & 0 & -M\end{pmatrix}\begin{pmatrix}l_f & l'_i & j\\ m_f & m'_i & m\end{pmatrix}\begin{pmatrix}l'_f & l_i & j\\ m'_f & m_i & m\end{pmatrix}, \tag{D15}$$

where the matrices are the Wigner 3-j symbols. We tested that both the approaches provide the same results.

[1] T. F. O'Malley, Theory of dissociative attachment, Phys. Rev. **150**, 14 (1966).

[2] J. N. Bardsley and F. Mandl, Resonant scattering of electrons by molecules, Rep. Prog. Phys. **31**, 471 (1968).

[3] A. Herzenberg, Oscillatory energy dependence of resonant electron-molecule scattering, J. Phys. B **1**, 548 (1968).

[4] W. Domcke and L. S. Cederbaum, On the interpretation of low-energy electron-HCl scattering phenomena, J. Phys. B: At. Mol. Phys. **14**, 149 (1981).

[5] L. S. Cederbaum and W. Domcke, Local against non-local complex potential in resonant electron-molecule scattering, J. Phys. B: At. Mol. Phys. **14**, 4665 (1981).

[6] W. Domcke and L. S. Cederbaum, Vibration-induced narrowing of electron scattering resonances near threshold, J. Phys. B: At. Mol. Phys. **13**, 2829 (1980).

[7] M. Čížek, J. Horáček, M. Allan, and W. Domcke, Resonances and threshold phenomena in low-energy electron collisions with hydrogen halides: New experimental and theoretical results, Czech. J. Phys. **52**, 1057 (2002).

[8] T. N. Rescigno, W. A. Isaacs, A. E. Orel, H.-D. Meyer, and C. W. McCurdy, Theoretical study of resonant vibrational excitation of CO_2 by electron impact, Phys. Rev. A **65**, 032716 (2002).

[9] C. W. McCurdy, W. A. Isaacs, H.-D. Meyer, and T. N. Rescigno, Resonant vibrational excitation of CO_2 by electron impact: Nuclear dynamics on the coupled components of the $^2\Pi_u$ resonance, Phys. Rev. A **67**, 042708 (2003).

[10] D. J. Haxton, Z. Zhang, H.-D. Meyer, T. N. Rescigno, and C. W. McCurdy, Dynamics of dissociative attachment of electrons to water through the $^2B_1$ metastable state of the anion, Phys. Rev. A **69**, 062714 (2004).

[11] D. J. Haxton, T. N. Rescigno, and C. W. McCurdy, Dissociative electron attachment to the H_2O molecule. II. Nuclear dynamics on coupled electronic surfaces within the local complex potential model, Phys. Rev. A **75**, 012711 (2007).

[12] S. T. Chourou and A. E. Orel, Dissociative electron attachment to HCN and HNC, Phys. Rev. A **80**, 032709 (2009).

[13] S. T. Chourou and A. E. Orel, Isotope effect in dissociative electron attachment to HCN, Phys. Rev. A **83**, 032709 (2011).

[14] H. B. Ambalampitiya and I. I. Fabrikant, Nonlocal complex potential theory of dissociative electron attachment: Inclusion of two vibrational modes, Phys. Rev. A **102**, 022802 (2020).

[15] H. Estrada, L. S. Cederbaum, and W. Domcke, Vibronic coupling of short–lived electronic states, J. Chem. Phys. **84**, 152 (1986).

[16] S. Feuerbacher, T. Sommerfeld, and L. S. Cederbaum, Intersections of potential energy surfaces of short-lived states: The complex analogue of conical intersections, J. Chem. Phys. **120**, 3201 (2004).

[17] S. Feuerbacher and L. S. Cederbaum, Jahn-Teller effect for short-lived states: Study of the complex potential energy surfaces, J. Chem. Phys. **121**, 5 (2004).

[18] J. Dvořák, M. Ranković, K. Houfek, P. Nag, R. Čurík, J. Fedor, and M. Čížek, Vibronic Coupling through the Continuum in the e+CO_2 System, Phys. Rev. Lett. **129**, 013401 (2022).

[19] M. A. Morrison, Interpretation of the near-threshold behavior of cross sections for e-CO_2 scattering, Phys. Rev. A **25**, 1445 (1982).

[20] K. H. Kochem, W. Sohn, N. Hebel, K. Jung, and H. Ehrhardt, Elastic electron scattering and vibrational excitation of CO_2 in the threshold energy region, J. Phys. B: At. Mol. Phys. **18**, 4455 (1985).

[21] L. A. Morgan, Virtual States and Resonances in Electron Scattering by CO_2, Phys. Rev. Lett. **80**, 1873 (1998).

[22] M. J. W. Boness and G. J. Schulz, Vibrational excitation in CO_2 via the 3.8-eV resonance, Phys. Rev. A **9**, 1969 (1974).

[23] B. L. Whitten and N. F. Lane, Near-threshold vibrational excitation in electron-CO_2 collisions: A simple model, Phys. Rev. A **26**, 3170 (1982).

[24] S. Mazevet, M. A. Morrison, L. A. Morgan, and R. K. Nesbet, Virtual-state effects on elastic scattering and vibrational excitation of CO_2 by electron impact, Phys. Rev. A **64**, 040701(R) (2001).

[25] H. Estrada and W. Domcke, On the virtual-state effect in low-energy electron-CO_2 scattering, J. Phys. B **18**, 4469 (1985).

[26] W. Vanroose, Z. Zhang, C. W. McCurdy, and T. N. Rescigno, Threshold Vibrational Excitation of CO_2 by Slow Electrons, Phys. Rev. Lett. **92**, 053201 (2004).

[27] I. Cadez, F. Gresteau, M. Tronc, and R. I. Hall, Resonant electron impact excitation of CO_2 in the 4 eV region, J. Phys. B: At. Mol. Phys. **10**, 3821 (1977).

[28] A. K. Kazansky and L. Y. Sergeeva, On the local theory of resonant inelastic collisions of slow electrons with carbon dioxide, J. Phys. B: At., Mol. Opt. Phys. **27**, 3217 (1994).

[29] A. Kazansky and L. Y. Sergeeva, A model study of vibrational excitation of carbon dioxide molecule by slow electrons: The role of wave packet sliding from the ridge, Z. Phys. D **37**, 305 (1996).

[30] D. G. Hopper, Analytic representation of the ground state potential surfaces for CO_2^- and CO_2. Implications for the O^-+ $CO \rightarrow CO_2^*+e$ chemiluminescent reaction and other related processes, Chem. Phys. **53**, 85 (1980).

[31] G. L. Gutsev, R. J. Bartlett, and R. N. Compton, Electron affinities of CO_2, OCS, and CS_2, J. Chem. Phys. **108**, 6756 (1998).

[32] T. N. Rescigno, D. A. Byrum, W. A. Isaacs, and C. W. McCurdy, Theoretical studies of low-energy electron-CO_2 scattering: Total, elastic, and differential cross sections, Phys. Rev. A **60**, 2186 (1999).

[33] J. Tennyson and L. A. Morgan, Electron collisions with polyatomic molecules using the R-matrix method, Phil. Trans. R. Soc. A. **357**, 1161 (1999).

[34] W. Vanroose, C. W. McCurdy, and T. N. Rescigno, Interpretation of low-energy electron-CO_2 scattering, Phys. Rev. A **66**, 032720 (2002).

[35] T. Sommerfeld, A fresh look at the $^2A_1$ CO_2^{2-} potential energy surface, J. Phys. B: At., Mol. Opt. Phys. **36**, L127 (2003).

[36] T. Sommerfeld, H.-D. Meyer, and L. S. Cederbaum, Potential energy surface of the CO_2^{2-} anion, Phys. Chem. Chem. Phys. **6**, 42 (2004).

[37] H. Köppel, W. Domcke, and L. S. Cederbaum, Theory of vibronic coupling in linear molecules, J. Chem. Phys. **74**, 2945 (1981).

[38] H. Köppel, W. Domcke, and L. S. Cederbaum, Multimode molecular dynamics beyond the Born-Oppenheimer approximation, in *Advances in Chemical Physics*, edited by I. Prigogine and S. A. Rice (John Wiley & Sons, New York, 1984), pp. 59–246

[39] H. Feshbach, A unified theory of nuclear reactions. II, Ann. Phys. **19**, 287 (1962).

[40] M. Čížek and K. Houfek, Nonlocal theory of resonance electron-molecule scattering, in *Low-Energy Electron Scattering from Molecules, Biomolecules and Surfaces*, edited by P. Čársky and R. Čurík (CRC Press, Boca Raton, FL, 2012), pp. 91–125.

[41] W. Domcke, Theory of resonance and threshold effects in electron-molecule collisions: The projection-operator approach, Phys. Rep. **208**, 97 (1991).

[42] W. J. Witteman, *The CO_2 Laser* (Springer-Verlag, Berlin, Heidelberg, 1987).

[43] A. Moradmand, D. S. Slaughter, D. J. Haxton, T. N. Rescigno, C. W. McCurdy, T. Weber, S. Matsika, A. L. Landers, A. Belkacem, and M. Fogle, Dissociative electron attachment to carbon dioxide via the $^2\Pi_u$ shape resonance, Phys. Rev. A **88**, 032703 (2013).

[44] D. Spence and G. J. Schulz, Temperature dependence of dissociative attachment in O_2 and CO_2, Phys. Rev. **188**, 280 (1969).

[45] G. Herzberg, *Molecular Spectra and Molecular Structure. Vol. 2, Infrared and Raman Spectra of Polyatomic Molecules* (Van Nostrand, New York, 1945).
[46] E. P. Wigner, On the behavior of cross sections near thresholds, Phys. Rev. **73**, 1002 (1948).
[47] R. J. Bieniek, Complex potential and electron spectrum in atomic collisions involving fast electronic transitions: Penning and associative ionization, Phys. Rev. A **18**, 392 (1978).
[48] M. Berman, H. Estrada, L. S. Cederbaum, and W. Domcke, Nuclear dynamics in resonant electron-molecule scattering beyond the local approximation: The 2.3-eV shape resonance in N_2, Phys. Rev. A **28**, 1363 (1983).
[49] R. Parini, cxroots: A Python module to find all the roots of a complex analytic function within a given contour (2018), https://github.com/rparini/cxroots.git.
[50] P. Kravanja and M. V. Barel, *Computing the Zeros of Analytic Functions* (Springer-Verlag, Berlin, 2000).
[51] T. H. Dunning, Gaussian basis sets for use in correlated molecular calculations. I. The atoms boron through neon and hydrogen, J. Chem. Phys. **90**, 1007 (1989).
[52] J. Tennyson, Electron-molecule collision calculations using the R-matrix method, Phys. Rep. **491**, 29 (2010).
[53] Z. Mašín, J. Benda, J. D. Gorfinkiel, A. G. Harvey, and J. Tennyson, Ukrmol+: A suite for modelling electronic processes in molecules interacting with electrons, positrons and photons using the R-matrix method, Comput. Phys. Commun. **249**, 107092 (2020).
[54] W. Domcke and C. Mündel, Calculation of cross sections for vibrational excitation and dissociative attachment in HCl and DCl beyond the local-complex-potential approximation, J. Phys. B: At. Mol. Phys. **18**, 4491 (1985).
[55] J. Horáček, M. Čížek, and W. Domcke, Generalization of the nonlocal resonance model for low-energy electron collisions with hydrogen halides: the variable threshold exponent, Theor. Chem. Acc. **100**, 31 (1998).
[56] D. M. Dennison, The infra-red spectra of polyatomic molecules. Part II, Rev. Mod. Phys. **12**, 175 (1940).
[57] H. Friedrich, *Scattering Theory* (Springer-Verlag, Berlin, Heidelberg, 2013).
[58] J. R. Taylor, *Scattering Theory: The Quantum Theory on Nonrelativistic Collisions* (Wiley, New York, 1972).
[59] H. Estrada and W. Domcke, Analytic properties of the S matrix for a simple model of fixed-nuclei electron-polar-molecule scattering, J. Phys. B: At. Mol. Phys. **17**, 279 (1984).
[60] M. Hestenes and E. Stiefel, Methods of conjugate gradients for solving linear systems, J. Res. Nat. Bur. Stand. **49**, 409 (1952).
[61] H. van der Vorst and J. Melissen, A Petrov-Galerkin type method for solving Axk = b, where A is symmetric complex, IEEE Trans. Magn. **26**, 706 (1990).
[62] T. Sogabe and S.-L. Zhang, A COCR method for solving complex symmetric linear systems, J. Comput. Appl. Math. **199**, 297 (2007), special Issue on Scientific Computing, Computer Arithmetic, and Validated Numerics (SCAN 2004).
[63] R. Fletcher, Conjugate gradient methods for indefinite systems, in *Numerical Analysis*, edited by G. A. Watson (Springer, Berlin, 1976), pp. 73–89.
[64] H. A. van der Vorst, Bi-CGSTAB: A fast and smoothly converging variant of Bi-CG for the solution of nonsymmetric linear systems, SIAM J. Sci. Stat. Comput. **13**, 631 (1992).
[65] S. F. Wong and G. J. Schulz, Vibrational Excitation in Benzene by Electron Impact via Resonances: Selection Rules, Phys. Rev. Lett. **35**, 1429 (1975).
[66] G. A. Gallup, Selection rules for vibrational energy loss by resonant electron impact in polyatomic molecules, Phys. Rev. A **34**, 2746 (1986).
[67] G. A. Gallup, Symmetry selection rules for vibrational excitation by resonant electron impact and a unified treatment of vibronic coupling between resonances and to the continuum: A complete symmetry analysis of vibrational excitation in benzene, J. Chem. Phys. **99**, 827 (1993).
[68] Roman Čurík, I. Paidarová, M. Allan, and P. Čársky, Joint experimental and theoretical study on vibrational excitation cross sections for electron collisions with diacetylene, J. Phys. Chem. A **118**, 9734 (2014).
[69] R. Čurík, P. Čársky, and M. Allan, Electron-impact vibrational excitation of cyclopropane, J. Chem. Phys. **142**, 144312 (2015).
[70] H. Bateman, On the numerical solution of linear integral equations, Proc. R. Soc. London A **100**, 441 (1922).
[71] K. Houfek, M. Čížek, and J. Horáček, Dissociative attachment of low-energy electrons to vibrationally excited hydrogen molecules, Czech. J. Phys. **52**, 29 (2002).
[72] C. Cohen-Tannoudji, B. Diu, and F. Laloë, *Quantum Mechanics, Volume 1: Basic Concepts, Tools, and Applications* (Wiley, New York, 2005).